Dissolution on Titan and on Earth: Towards the age of Titan's landscapes

Thomas Cornet, Daniel Cordier, T. Le Bahers, Olivier Bourgeois, Cyril Fleurant, Stéphane Le Mouélic, Nicolas Altobelli

AGU PUBLICATIONS

JGR

Journal of Geophysical Research: Planets

RESEARCH ARTICLE

10.1002/2014JE004738

Key Points:
- Titan's lacustrine depressions result from the dissolution of the surface
- Denudation rates allow to infer dissolution timescales on Earth and Titan
- Titan's depressions developed in less than a few hundred million years

Correspondence to:
T. Cornet,
tcornet@sciops.esa.int

Citation:
Cornet, T., D. Cordier, T. Le Bahers, O. Bourgeois, C. Fleurant, S. Le Mouélic, and N. Altobelli (2015), Dissolution on Titan and on Earth: Toward the age of Titan's karstic landscapes, *J. Geophys. Res. Planets*, *120*, 1044–1074, doi:10.1002/2014JE004738.

Received 3 OCT 2014
Accepted 19 APR 2015
Accepted article online 25 APR 2015
Published online 4 JUN 2015

Dissolution on Titan and on Earth: Toward the age of Titan's karstic landscapes

Thomas Cornet[1], Daniel Cordier[2], Tangui Le Bahers[3], Olivier Bourgeois[4], Cyril Fleurant[5], Stéphane Le Mouélic[4], and Nicolas Altobelli[1]

[1]European Space Agency (ESA), European Space Astronomy Centre (ESAC), Villanueva de la Canada, Spain, [2]Institut UTINAM, CNRS/INSU, Université de Franche-Comté, Besançon Cedex, France, [3]Laboratoire de Chimie UMR 5182, Université de Lyon, Université Claude Bernard Lyon 1, ENS Lyon, Lyon, France, [4]LPG Nantes, UMR 6112, CNRS, OSUNA, Université de Nantes, 2 rue de la Houssinière, Nantes, France, [5]LETG - UMR CNRS 6554, Université d'Angers, UFR Sciences, Angers, France,

Abstract Titan's polar surface is dotted with hundreds of lacustrine depressions. Based on the hypothesis that they are karstic in origin, we aim at determining the efficiency of surface dissolution as a landshaping process on Titan, in a comparative planetology perspective with the Earth as reference. Our approach is based on the calculation of solutional denudation rates and allow inference of formation timescales for topographic depressions developed by chemical erosion on both planetary bodies. The model depends on the solubility of solids in liquids, the density of solids and liquids, and the average annual net rainfall rates. We compute and compare the denudation rates of pure solid organics in liquid hydrocarbons and of minerals in liquid water over Titan and Earth timescales. We then investigate the denudation rates of a superficial organic layer in liquid methane over one Titan year. At this timescale, such a layer on Titan would behave like salts or carbonates on Earth depending on its composition, which means that dissolution processes would likely occur but would be 30 times slower on Titan compared to the Earth due to the seasonality of precipitation. Assuming an average depth of 100 m for Titan's lacustrine depressions, these could have developed in a few tens of millions of years at polar latitudes higher than 70°N and S, and a few hundreds of million years at lower polar latitudes. The ages determined are consistent with the youth of the surface (<1 Gyr) and the repartition of dissolution-related landforms on Titan.

1. Introduction

Along with the Earth, Saturn's icy moon Titan is the only planetary body of the entire solar system that possesses lakes and seas [*Lopes et al.*, 2007; *Stofan et al.*, 2007; *Hayes et al.*, 2008]. Some of these lakes and seas are currently covered by liquids, while others are not [*Hayes et al.*, 2008]. Most are located in the polar regions [*Hayes et al.*, 2008; *Aharonson et al.*, 2009], although a few occurrences have been reported at lower latitudes [*Moore and Howard*, 2010; *Vixie et al.*, 2012]. The currently filled lakes and seas are located poleward of 70° of latitude in both hemispheres whereas most empty depressions are located at lower latitudes (Figure 1) [*Hayes et al.*, 2008; *Aharonson et al.*, 2009].

Altogether, empty depressions, lakes, seas, and fluvial channels argue for the presence of an active "hydrological" cycle on Titan similar to that of the Earth, with exchanges between the subsurface (ground liquids), the surface (lakes, seas, and fluvial channels), and Titan's methane-rich atmosphere, where convective clouds and sporadic intense rainstorms have been imaged by the Cassini spacecraft instruments [*Turtle et al.*, 2011a]. Methane, rather than water as on Earth, probably dominates the cycle on Titan [*Lunine et al.*, 2008] and thus constitutes one of the main components of the surface liquid bodies observed in the polar regions [*Glein and Shock*, 2013; *Tan et al.*, 2013]. Ethane, the main photodissociation product of methane [*Atreya*, 2007], is also implied in Titan's lakes chemistry, as predicted by several thermodynamical models [*Lunine et al.*, 1983; *Raulin*, 1987; *Dubouloz et al.*, 1989; *Cordier et al.*, 2009; *Tan et al.*, 2013; *Cordier et al.*, 2013a; *Glein and Shock*, 2013], or as identified in Ontario Lacus thanks to the Cassini Visual and Infrared Mapping Spectrometer (VIMS) instrument [*Brown et al.*, 2008].

Titan's lakes are located in topographic depressions carved into the ground by geological processes that are poorly understood to date. The origin of the liquid would be related to precipitation, surface runoff, and underground circulation, leading to the accumulation of liquids in local topographic depressions.

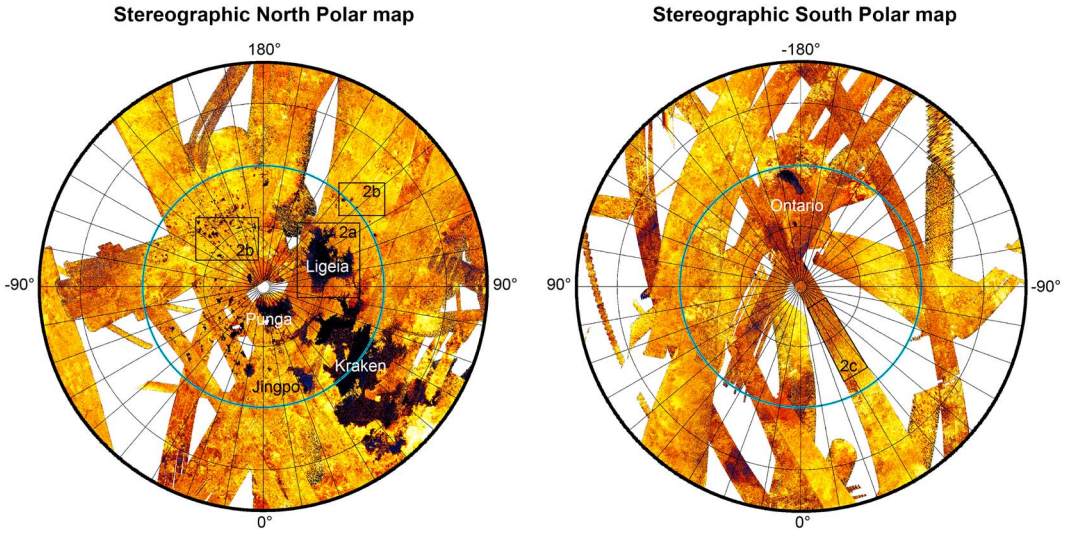

Figure 1. RADAR Synthetic Aperture Radar (SAR) mosaic of the TA (2004) to T95 (2013) flybys in north and south polar stereographic projections (down to 55° latitudes). All current lakes observed to date are located above 70° in latitude (blue circles).

In the present work, we aim to constrain the origin and the age of these depressions. Section 2 first provides a brief overview of their geology and a discussion of their possible origin based on their morphological characteristics and from considerations about Titan's surface composition and climate. Based on this discussion, we propose a new quantitative model, whereby the depressions have formed by the dissolution of a surface geological layer over geological timescales, such as in karstic landscapes on Earth.

In terrestrial karstic landscapes, the maximum quantity of mineral that can be dissolved per year, namely the solutional denudation rate, can be computed using a simple thermodynamics-climatic model presented in section 3. The denudation rate depends on the nature of the surface material (solubility and density of the minerals) and on the climate conditions (precipitation, evaporation, and surface temperature). Using this simple model, it is possible to determine theoretical timescales for the formation of specific karstic landforms on Earth, which are compared to relative or absolute age determinations in section 4.

We apply the same model to Titan's surface in section 5. Section 5.1 is dedicated to the comparative study of denudation rates of pure solid organics in pure liquid methane, ethane, and propane and of common soluble minerals (halite, gypsum, anhydrite, calcite, and dolomite), cornerstones of karstic landscapes development on Earth, in liquid water over terrestrial timescales. Section 5.2 describes the computation of denudation rates of pure solids and of mixed organic surface layers in liquid methane over Titan timescales by using the methane precipitation rates extracted from the Global Circulation Model (GCM) of *Schneider et al.* [2012]. Based on these denudation rates, we compute the timescales needed to develop the typical 100 m deep topographic depressions observed in the polar regions of Titan (section 6) and compare them to timescales estimated from other observations (e.g., crater counting and dune formation).

2. Geology of Titan's Lacustrine Depressions

2.1. Geomorphological Settings

Seas and lacustrine depressions strongly differ in shape (Figure 2). On the one hand, seas are large (several hundred kilometers in width) and deep (from 150 to 300–400 m in depth) [*Lorenz et al.*, 2008, 2014; *Mastrogiuseppe et al.*, 2014]. They possess dendritic contours and are connected to fluvial channels (e.g., Ligeia Mare, Figure 2a) [*Stofan et al.*, 2007; *Sotin et al.*, 2012; *Wasiak et al.*, 2013]. They seem to develop in areas associated with reliefs, which constitute some parts of their coastlines.

On the other hand, Titan's lacustrine depressions (Figure 2b) develop in relatively flat areas. They lie between 300 and 800 m above the level of the northern seas [*Stiles et al.*, 2009; *Kirk et al.*, 2012]. They are typically rounded or lobate in shape, and some of them seem to be interconnected [*Bourgeois et al.*, 2008]. Their widths vary from a few tens of kilometers, such as for most of Titan's lacunae, up to a few hundred kilometers, such as Ontario Lacus or Jingpo Lacus. Their depths have been tentatively estimated to range from a few meters

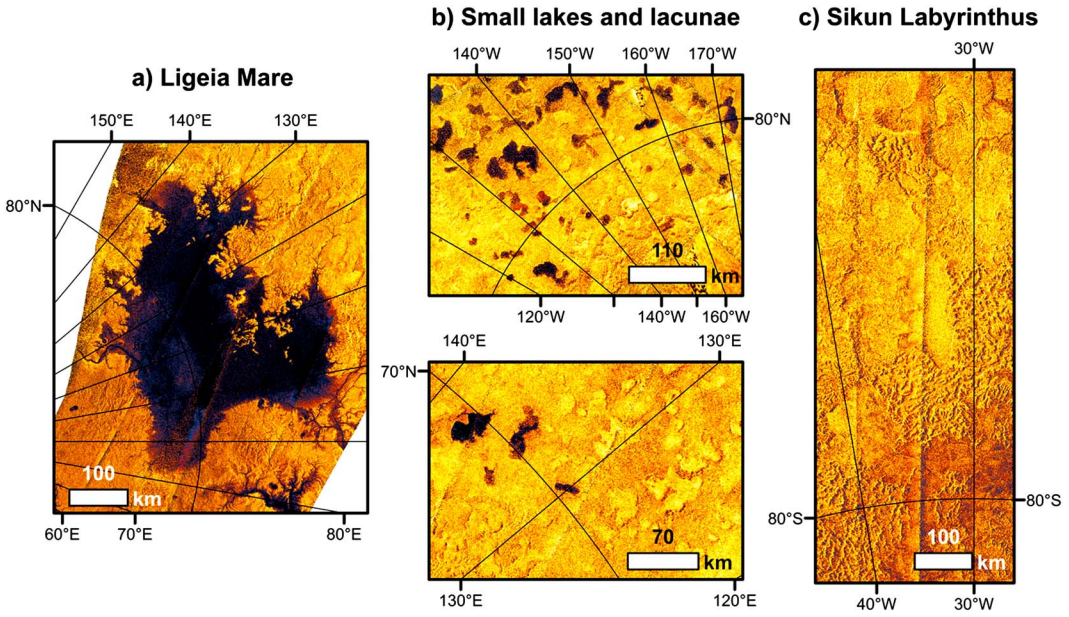

Figure 2. RADAR SAR views of (a) Titan's second largest sea Ligeia Mare, (b) empty and liquid-covered lacustrine depressions, and (c) the heavily dissected terrains of Sikun Labyrinthus. Ligeia Mare clearly differs in size and shape from the smaller lacustrine depressions, which suggests a different formation mechanism. Lacustrine depressions and labyrinthic terrains pertain to the class of features potentially related to the dissolution of the surface.

to 100–300 m [*Hayes et al.*, 2008; *Kirk and Howington-Kraus*, 2008; *Stiles et al.*, 2009; *Lorenz et al.*, 2013], with "steep"-sided walls [*Mitchell et al.*, 2007; *Bourgeois et al.*, 2008; *Kirk and Howington-Kraus*, 2008; *Hayes et al.*, 2008]. The liquid-covered depressions would lie 250 m below the floor of the empty depressions [*Kirk et al.*, 2007], which could be indicative of the presence of an alkanofer in the subsurface, analog to terrestrial aquifers, filling or not the depressions depending on their base level [*Hayes et al.*, 2008; *Cornet et al.*, 2012]. The depressions sometimes possess a raised rim, ranging from a few hundred meters up to 600 m in height [*Kirk et al.*, 2007; *Kirk and Howington-Kraus*, 2008]. All these numbers are likely subject to modification following future improvements in depth-deriving techniques.

2.2. Geological Origin of the Depressions

The geological origin of the topographic depressions and how they are fed by liquids are still debated. The geometric analysis of the lakes by *Sharma and Byrne* [2010, 2011] led to the conclusion that, unlike on Earth, the formation mechanism of the lacustrine depressions cannot be derived from the analysis of their coastline shapes. Recently, *Black et al.* [2012] and *Tewelde et al.* [2013] showed that mechanical erosion due to fluvial activity would have a minor influence in landscape evolution on Titan. Given this context, several hypotheses are being explored to understand how Titan's lakes have formed. These include (1) cryovolcanic origin [*Mitchell et al.*, 2007; *Wood et al.*, 2007], forming topographic depressions in which lakes can exist, such as in terrestrial calderas [*Acocella*, 2007] or maars [*Lorenz*, 1986]; (2) thermokarstic origin [*Kargel et al.*, 2007; *Mitchell et al.*, 2007; *Harrisson*, 2012], where the cyclic destabilization of a methane frozen ground would form topographic depressions, such as in periglacial areas on Earth where the permafrost cyclically freezes and thaws and forms thermokarst lakes, pingos, or alases [*French*, 2007]; and (3) solutional origin [*Mitchell et al.*, 2007; *Bourgeois et al.*, 2008; *Mitchell*, 2008; *Mitchell and Malaska*, 2011; *Malaska et al.*, 2011; *Barnes et al.*, 2011; *Cornet et al.*, 2012], where processes analogous to terrestrial karstic dissolution create topographic depressions, such as terrestrial sinkholes/dolines, playas, and pans under various climates [*Shaw and Thomas*, 2000; *Ford and Williams*, 2007].

On the one hand, the general lack of unequivocal cryovolcanic features on Titan tends to limit the likelihood of the cryovolcanic hypothesis [*Moore and Pappalardo*, 2011]. A methane-based permafrost would be difficult to form on Titan due to the presence of nitrogen in the atmosphere [*Lorenz and Lunine*, 2002; *Heintz and Bich*, 2009]. Its putative cyclic destabilization would also be challenging, given the tiny temperature variations between summer and winter, day and night, and equator and poles [*Jennings et al.*, 2009; *Lora et al.*, 2011; *Cottini et al.*, 2012] over all timescales [*Aharonson et al.*, 2009; *Lora et al.*, 2011]. On the other hand, solid organics have been shown to be quite soluble in liquid hydrocarbons under Titan's surface conditions [*Lunine et al.*,

Table 1. Production Rates (in Molecules/cm^2/s) of Simple Solid Organics in Titan's Atmosphere Derived From Several Photochemical Models[a]

	Y84	T95	L96	W04	L08	K09
C_2H_6	5.80×10^9	1.50×10^{10}	1.41×10^9	1.60×10^9	4.10×10^9	1.16×10^9
C_3H_8	1.40×10^8	5.40×10^8	3.14×10^7	3.30×10^7	3.70×10^8	2.17×10^8
C_4H_{10}	2.30×10^7	8.80×10^7		3.00×10^7		7.02×10^5
C_2H_2	1.20×10^9	1.10×10^9	9.28×10^8	3.70×10^8	3.20×10^8	3.22×10^8
C_2H_4				9.30×10^7	6.00×10^7	
C_3H_4						2.64×10^6
C_4H_4						1.57×10^4
C_4H_6				6.50×10^4		1.71×10^7
C_6H_6				4.60×10^5	2.10×10^5	1.08×10^6
HCN	2.00×10^8	1.00×10^8	8.00×10^7	2.10×10^6	3.20×10^8	1.54×10^8
HC_3N	1.70×10^7		3.73×10^7	1.30×10^7	9.20×10^6	1.26×10^7
C_2N_2	1.20×10^7		2.89×10^4	2.00×10^6	2.60×10^4	3.52×10^6
C_4N_2			7.20×10^6	9.70×10^5	1.90×10^6	
CH_3CN			6.61×10^5	3.40×10^4	1.70×10^7	1.27×10^7
C_2H_3CN				1.60×10^7	2.80×10^5	1.62×10^7
C_2H_5CN						8.00×10^5

[a]Not reported here is the production rate of tholins, estimated by *Cabane et al.* [1992], *Rannou et al.* [2003], and *Krasnopolsky* [2009] to be between 0.2 and 7 kg/cm^2/GEyr (giga Earth year). The list of compound names is available in Appendix A. Y84: *Yung et al.* [1984], T95: *Toublanc et al.* [1995], L96: *Lara et al.* [1996], W04: *Wilson and Atreya* [2004], L08: *Lavvas et al.* [2008a, 2008b], K09: *Krasnopolsky* [2009].

1983; *Raulin*, 1987; *Dubouloz et al.*, 1989; *Cordier et al.*, 2009, 2013a, 2013b; *Glein and Shock*, 2013; *Tan et al.*, 2013], provided that they are available at the surface. The observation of bright terrain around present lakes and inside of empty depressions, analogs of terrestrial evaporites produced by the evaporitic crystallization of dissolved solids, also strengthens this hypothesis [*Barnes et al.*, 2011; *MacKenzie et al.*, 2014].

On Earth, dissolution-related landforms are not restricted to sinkholes/dolines, pans, or playa, which characterize relatively young karsts [*Ford and Williams*, 2007]. Spectacular instances of reliefs nibbled by dissolution, known as cone/cockpit karsts, fluvio karsts, or tower karsts, exist under temperate to tropical/equatorial climates, such as in China [*Xuewen and Weihai*, 2006; *Waltham*, 2008], Indonesia [*Ford and Williams*, 2007], or the Caribbeans [*Fleurant et al.*, 2008; *Lyew-Ayee*, 2010]. The observation of possible mature karst-like terrains in Sikun Labyrinthus (Figure 2c) by *Malaska et al.* [2010], similar to these terrestrial karstic landforms also gives further credence to the hypothesis that lacustrine depressions on Titan are karstic in origin.

2.3. Composition of Titan's Solid Surface

Titan's surface can be divided into five main spectral units identified by the Cassini/VIMS instrument: bright terrain, dark equatorial dune fields, or dark brown units, blue units, 5 μm bright units, and the dark lakes [*Barnes et al.*, 2007; *Stephan et al.*, 2009]. In the polar regions, the solid surface appears dominantly as bright terrain, lakes, and patches identified as the 5 μm bright unit in VIMS data [*Barnes et al.*, 2011; *Sotin et al.*, 2012; *MacKenzie et al.*, 2014]. The spectral characteristics of the VIMS 5 μm bright unit seen inside and around some polar (and equatorial) lacustrine depressions indicate the presence of various hydrocarbons and nitriles [*Clark et al.*, 2010; *Moriconi et al.*, 2010] and are not compatible with the presence of water ice [*Barnes et al.*, 2009].

The origin of the organic materials is probably linked to the atmospheric photochemistry, which results in the formation of various hydrocarbons and nitriles [*Lavvas et al.*, 2008a, 2008b; *Krasnopolsky*, 2009] detected by Cassini [*Cui et al.*, 2009; *Magee et al.*, 2009; *Clark et al.*, 2010; *Coustenis et al.*, 2010; *Vinatier et al.*, 2010; *Cottini et al.*, 2012]. Table 1 gives the estimated fluxes of some produced organics, as derived from several models. Most of these compounds could condense as solids and sediment onto the surface over geological timescales [*Atreya*, 2007; *Malaska et al.*, 2011]. Most of them would be relatively soluble in liquid alkanes [*Raulin*, 1987; *Dubouloz et al.*, 1989; *Cordier et al.*, 2009, 2013a; *Glein and Shock*, 2013; *Tan et al.*, 2013].

It is therefore reasonable to assume that a superficial soluble layer, composed of organic products, exists at the surface of Titan. Episodic dissolution of this layer would be responsible for the development of karst-like depressions and labyrinthic terrains [*Bourgeois et al.*, 2008; *Malaska et al.*, 2010, 2011; *Mitchell and Malaska*, 2011; *Cornet et al.*, 2012]. Evaporitic crystallization could also occur after episodes of dissolution in the liquids, forming evaporite-like deposits [*Barnes et al.*, 2011; *Cornet et al.*, 2012; *Cordier et al.*, 2013b; *MacKenzie et al.*, 2014].

3. Solutional Denudation Rates on Earth

On Earth, karstic landforms develop thanks to the dissolution of carbonate (calcite and dolomite) and evaporite (gypsum, anhydrite and halite) minerals under the action of groundwater and rainfall percolating through pore space and fractures present in rocks. The mineral solubilities vary as a function of the environmental conditions (amount of rain and partial pressure of carbon dioxide) [*Ford and Williams*, 2007]. Karstic landforms like dolines or sinkholes are often located under temperate to humid climates in carbonates (though gypsum or halite karsts also exist on Earth). They reach depths of up to a few hundred meters [*Ford and Williams*, 2007]. Karsto-evaporitic landforms like pans are located under semiarid to arid climates. They reach depths of up to a few tens of meters [*Goudie and Wells*, 1995; *Bowen and Johnson*, 2012]. Evaporitic landforms like playas are located under arid climates. They are characterized by their extreme flatness and can occur in any kind of topographic depression [*Shaw and Thomas*, 2000].

Denudation rates (hereafter *DR*) in terrestrial karstic landscapes are primarily constrained by geological (age and physicochemical nature of rocks) and climate (net precipitation rates evolution) analyses. For many limestone-dominated areas (the majority of karst areas), it is commonly assumed that dissolution features are mainly created in the epikarstic zone located in the top few meters below the surface [*White*, 1984; *Ford and Williams*, 2007]. Classically, in karstic terrains, the chemical/solutional denudation rate *DR* (in meters per Earth year or m/Eyr) is related to the rock physicochemical properties and the climate by the following equation [*White*, 1984; *Tucker et al.*, 2001; *Ford and Williams*, 2007; *Fleurant et al.*, 2008]:

$$DR = \rho_w \frac{M_{\text{calcite}}}{\rho_{\text{calcite}}} \tau\, m_{\text{Ca}} \qquad \text{(m/Eyr)}, \tag{1}$$

where ρ_w is the mass density of liquid water ($\simeq$ 1000 kg/m^3), M_{calcite} is the molar mass of calcite (in kg/mol), ρ_{calcite} is the mass density of calcite (in kg/m^3), τ is the mean annual net precipitation rate (in m/yr), equivalent to the sum of runoff and infiltration or the difference between precipitation and evapotranspiration over long timescales [*White*, 2012], and m_{Ca} is the equilibrium molality of calcite (Ca^{2+} cations, in mol/kg), assuming an instantaneous dissolution. Following this equation, denudation rates depend linearly on the climate precipitation regime and on the molality of dissolved materials.

Molality calculations are provided in Appendix B for various soluble minerals, based on two thermodynamic hypotheses: an Ideal Solution Theory (IST, no preferential interactions between molecules) and an Electrolyte Solution Theory (EST, preferential interactions between molecules). We incorporated the effect of CO_2 gas dissolved in water, which acidifies water due to a series of intermediate reactions (one of which producing carbonic acid) and increases the dissolution rates of carbonates (calcite and dolomite, see Appendix B for more details). The partial pressure of CO_2 (hereafter P_{CO_2}, in atm) under different climates can be computed as follows [*Ford and Williams*, 2007]:

$$\log P_{CO_2} = -3.47 + 2.09\,(1 - e^{-0.00172\,AET}), \tag{2}$$

where *AET* is the mean annual evapotranspiration rate in mm/Eyr. Applying the above formula gives $P_{CO_2} < 3$ matm for arid areas, $3 < P_{CO_2} < 12$ matm for temperate areas and $P_{CO_2} > 12$ matm for tropical or equatorial climates. The resulting typical values of denudation rates on Earth for common soluble minerals in liquid water are given in Table 2. Depending on the climatic conditions, denudation rates of salts are on the order of a few hundred μm to a few centimeters per Earth year, whereas denudation rates of carbonates are on the order of a few μm to a few hundred μm per Earth year. Note that chemical erosion is just one of the landshaping processes on Earth. Other mechanisms, such as mechanical erosion, would tend to increase the total denudation rate of a surface [*Fleurant et al.*, 2008]. The dissolved solids can take part in the crystallization

Table 2. Solutional Denudation Rates in mm/Eyr for Terrestrial Minerals at 298.15 K and Under Various Climatic Conditions (CO_2 Content and Precipitation Rates)[a]

Name	τ = 30 cm/Eyr	τ = 1 m/Eyr
	Dissolution by Dissociation	
Halite	50.643	167.122
Gyspum	0.504	1.662
Anhydrite	0.224	0.740
Calcite	8.55×10^{-4}	2.82×10^{-3}
Dolomite	7.84×10^{-4}	2.59×10^{-3}
	Acid Dissolution	
Calcite, P_{CO_2} = 0.33 matm	0.006	0.020
Dolomite, P_{CO_2} = 0.33 matm	0.005	0.017
Calcite, P_{CO_2} = 0.01 atm	0.020	0.066
Dolomite, P_{CO_2} = 0.01 atm	0.017	0.057
Calcite, P_{CO_2} = 0.11 atm	0.047	0.156
Dolomite, P_{CO_2} = 0.11 atm	0.040	0.132

[a]All values correspond to the EST hypothesis except those for halite (IST).

of soluble deposits at the surface (e.g., calcretes or salt crusts in arid environments) or in the subsurface (e.g., cements), when they saturate the liquids. They do not necessarily crystallize at the location where they dissolved [*Ford and Williams*, 2007].

4. Denudation Rates to Determine Ages of Terrestrial Karstic Landscapes

Using the denudation rates, theoretical timescales for the development of dissolution landforms of a given depth can be inferred. We test hereafter this hypothesis on terrestrial instances by comparing ages determined from the denudation rates and ages determined from relative or absolute chronology. For carbonates, the partial pressure of CO_2 is computed based on the MOD16 Global Evapotranspiration Product of the University of Montana/Environmental Systems Research Institute Mapping Center. The notation GEyrs, MEyrs, and kEyrs will refer to timescales expressed, respectively, in giga Earth years (10^9 years), million Earth years (10^6 years), and kilo Earth years (10^3 years) in the following sections.

4.1. Example Under a Hyperarid Climate: The Caves of the Mount Sedom Diapir (Israel)

Mount Sedom is a 11×1.5 km salt diapir located in Israel, 250 m above the level of the Dead sea, under a hyperarid climate [*Frumkin*, 1994, 1996]. It is composed of a Pliocene-Pleistocene (<7 MEyrs) halite basis covered by a 5–50 m thick layer composed of anhydrite and sandstones. Several sinkholes and caves exist in Mount Sedom [*Frumkin*, 1994].

In this part of Israel, the present-day hyperarid climate leads to average rainfall rates of 50 mm/Eyr, of which 10–15 mm/Eyr constitutes the average effective rainfall rate (τ). Gvishim and Mishquafaim Caves are, respectively, 60 m and 20 m deep caves and are essentially carved into halite in the northern part of Mount Sedom. Radioisotopic age measurements in several caves of Mount Sedom give an Holocene age, about 8 kEyrs (and around 3.2–3.4 kEyrs from age measurements performed in Mishquafaim Cave) [*Frumkin*, 1996].

Assuming that underground dissolution is somewhat connected to the rainfall percolating through anhydrite and reaching halite, the denudation rates computed with our model (equation (1)) over this region are $DR \simeq 1.69 - 2.53$ mm/Eyr. The timescales required to form these caves would be between 23.7 and 35.5 kEyrs for Gvishim Cave, and between 7.9 and 11.8 kEyrs for Mishquafaim Cave, longer than those estimated from radioisotopic measurements.

However, it should be noted that Mount Sedom experiences a rather deep dissolution, the load of dissolved solids in the underground liquid water flowing in its caves being up to 3 times that of surface runoff [*Frumkin*, 1994]. Therefore, considering that the denudation rate should be 3 times greater, we find timescales of development between 7.9 and 11.8 kEyrs for Gvishim Cave and between 2.6 and 3.9 kEyrs for Mishquafaim Cave, in better agreement with age measurements.

4.2. Example Under a Semiarid Climate: The Etosha Super-Pan (Namibia)

The Etosha Pan, located in Namibia under a semiarid climate, is a flat 120×60 km karsto-evaporitic depression that has already been suggested as a potential analog for Titan's lacustrine depressions [*Bourgeois et al.*, 2008; *Cornet et al.*, 2012]. The depression is about 15 to 20 m deep at most and has been carved into the carbonate layer essentially composed of calcretes and dolocretes lying on top a middle Tertiary-Quaternary detritical

sedimentary sequence that covers the Owambo basin [*Buch and Rose*, 1996; *Hipondoka*, 2005]. This sedimentary sequence is believed to have accumulated under a semiarid climate, relatively similar to the current one. The age of the calcrete layer is not known precisely, but its formation is believed to have started during the Miocene/Pliocene transition about 7 MEyrs ago [*Buch*, 1997; *Buch and Trippner*, 1997], or even later during the late Pliocene, 4 MEyrs ago [*Miller et al.*, 2010]. The Etosha Pan is believed to have developed at the expense of the calcrete layer since 2 MEyrs [*Miller et al.*, 2010].

In the Owambo sedimentary basin, $AET \simeq 350$ mm/Eyr, yielding $P_{CO_2} = 3$ matm. Precipitation rates during the summer rainy season reach up to 500 mm/Eyr, which leads to $\tau = 150$ mm/Eyr at most. These conditions lead to $DR = 6.5$ μm/Eyr in a substratum composed of calcite (calcrete) and $DR = 5.6$ μm/Eyr in a substratum composed of dolomite (dolocrete). These denudation rates give an approximate age for the Etosha Pan of about 2.31–3.08 MEyrs in calcretes and 2.68 to 3.57 MEyrs in dolocretes. These ages are consistent with ages estimated from geological observations (< 4 MEyrs).

4.3. Example Under a Temperate Climate: The Doline of Crveno Jezero (Croatia)

Crveno Jezero is a 350 m wide collapse doline located in the Dinaric Karst of Croatia, under a presently Mediterranean temperate climate. This part of the Dinaric Karst is essentially composed of limestones and dolomites that have been deposited during the Mesozoic (Triassic to Cretaceous), when the area was covered by shallow marine carbonate shelves [*Vlahovic et al.*, 2002; *Mihevc et al.*, 2010]. The cliffs forming the doline are up to 250 m in height. The bottom of the depression is covered by a lake, named Red Lake, about 250 m deep. The total depth of the doline is therefore about 500 m [*Garasic*, 2001, 2012].

Although the formation process of the collapse dolines in the area is still not completely understood, especially in terms of the relative importance and timing of the collapse compared to the dissolution in the development of the structure, the uplift linked to the formation of the Alps (Eocene–Oligocene) led to the exposure of these carbonates and their subsequent karstification since at least Oligo-Miocene times (last 30 MEyrs) [*Sket*, 2012]. At some point, dissolution occurred to form an underground cave; then the load of the capping rocks exceeded their cohesion, leading to the brutal or progressive collapse of the cap in the empty space beneath. The timescale calculated for the doline formation therefore constitutes a higher estimate. Age determinations in the northern Dinaric caves have been performed and show that karstification would be older than 4 to 5 MEyrs [*Zupan Hajna*, 2012]. Crveno Jezero thus developed between 4 and 30 MEyrs ago.

In this region of Croatia, $AET \simeq 500$ mm/Eyr, which leads to $P_{CO_2} = 5.44$ matm. Annual mean precipitation rates are about 1100 mm/Eyr [*Mihevc et al.*, 2010], leading to $\tau = 600$ mm/Eyr. These parameters give $DR = 31.8$ μm/Eyr in limestones dominated by calcite ($DR = 27.5$ μm/Eyr in limestones dominated by dolomite). The time required to dissolve 500 m of calcite under these present conditions would be around 15.7 MEyrs (18.2 MEyrs in dolomite). It is likely that cap rocks fell into the cave, leading to a younger age (1 m of calcite and dolomite dissolve in about 31 and 36 kEyrs, respectively). However, the age determined by our method is still consistent with the geological records.

4.4. Example Under a Tropical Climate: The Xiaozhai Tiankeng (China)

The Xiaozhai Tiankeng is a 600 m wide collapse doline located in the Chongqing province of China, under a tropical climate. The depth of this doline is evaluated between 511 and 662 m depending on the location [*Xuewen and Weihai*, 2006; *Ford and Williams*, 2007]. It is organized into two major collapse structures, an upper 320 m deep structure and a lower 342 m deep shaft. The tiankeng developed into Triassic limestones in a karst drainage basin. It results from various surface and subsurface processes such as dissolution, fluid flows, and collapse. Tiankengs of China would have formed during the late Pleistocene (last 128,000 Eyrs) [*Xuewen and Weihai*, 2006] under an equatorial monsoonal climate similar to nowadays, emplaced 14 MEyrs ago [*Wang and Li*, 2009].

In the area, annual precipitation rates are about 1500 mm/Eyr, for an annual evapotranspiration rate of about 800 mm/Eyr, which leads to $P_{CO_2} = 0.0123$ atm and $\tau = 700$ mm/Eyr. Under these conditions, $DR = 49.6$ μm/Eyr (calcite) or $DR = 42.6$ μm/Eyr (dolomite) and the timescale to form the Xiaozhai Tiankeng would be between 10.3 and 13.3 MEyrs (calcite) and 12.0 and 15.5 MEyrs (dolomite), considerably longer timescales than those estimated from geological records. However, such a difference is to be expected, since the formation of gigantic tiankengs are subject to complex interconnected surface processes not taken into account in these simple calculations (collapse and underground circulation of water). This illustrates the limits of our method, generally overestimating the ages of karstic features when they do not result from dissolution only.

5. Denudation Rates on Titan

Equation (1) has to be adapted for Titan. From thermodynamics, we compute molar volumes ($V_{m,i}$ in m^3/mol, see Appendix C) and mole fractions at saturation ($X_{i,sat}$, see Appendix B) instead of mass densities and molalities. We considered the Ideal and the nonideal Regular Solutions Theories (IST and RST, respectively) and ensured that our results are consistent with experimentally determined solubilities. The RST has been developed to determine the solubility of nonpolar to slightly polar molecules, such as simple hydrocarbons or carbon dioxide, in nonpolar solvents. It is less likely to be appropriate for polar molecules such as nitriles/tholins and water ice. We therefore always provide a comparison between the IST and the RST in order to assess the uncertainty of the calculation by using the RST for polar molecules (see also Appendix B). However, we consider the RST, which provides our lowest and more realistic solubilities (at least for hydrocarbons), as the most suited model for the study. We assume that dissolution is instantaneous, which is not unreasonable given the rapid saturation of solid hydrocarbons in liquid ethane inferred from recent dissolution experiments [*Malaska and Hodyss*, 2014], compared to the long geological timescales considered in our work. For a binary solute-solvent system, equation (1) becomes

$$DR_i = \frac{X_{i,\mathrm{sat}}}{1 - X_{i,\mathrm{sat}}} \tau \frac{V^S_{\mathrm{m},i}}{V^L_{\mathrm{m,solv}}} \qquad \text{(m/Eyr)}, \tag{3}$$

where $V^S_{\mathrm{m},i}$ and $V^L_{\mathrm{m,\,solv}}$ are the molar volumes of the solid (crystallized) phase and of the liquid phase, respectively.

5.1. Comparison Between Titan and the Earth Over Terrestrial Timescales

In order to compare the behavior of Titan's solids in Titan's liquids with that of minerals in liquid water on Earth, we computed Titan's and Earth's denudation rates over Earth timescales by varying the precipitation rate between 0 and 2 m/Eyr. This range of precipitation rates encompasses the expected range on Titan (up to 1.2–1.3 m/Eyr during the rainy season [*Schneider et al.*, 2012]). It also covers the precipitation range between arid and tropical climates on Earth. This comparison is illustrated in Figures 3 (for hydrocarbons and carbon dioxide ice) and 4 (for nitriles and water ice), for which we fixed Titan's temperature to 91.5 K (the surface temperature during the rainy season according to *Schneider et al.* [2012]) and Earth's temperature to 298.15 K (with a partial pressure of carbon dioxide equal to 0.33 matm).

All organic compounds except $C_{11}H_{11}N$ would behave like common mineral salts (halite, gypsum, or anhydrite) according to the IST, which means that they would experience dissolution rates in the range of hundred μm to a few centimeters over one Eyr. According to the RST and assuming that the liquid is methane, C_2H_4 would behave like halite (centimeter-scale dissolution); C_4H_{10} and C_4H_4 like gypsum (hundred μm to millimeter-scale dissolution); C_2H_2, C_3H_4, C_4H_6, and CO_2 like carbonates (up to hundred μm-scale dissolution). C_6H_6 and nitriles would be less soluble in methane than calcite is in pure liquid water, with the least soluble nitriles being $C_{11}H_{11}N$, HCN, and CH_3CN. As expected, water ice is completely insoluble according to the RST, developed for nonpolar molecules.

The denudation rates of all organic compounds are higher in ethane and propane than in methane. Nitriles and C_6H_6, which are poorly soluble in methane, are quite soluble in ethane and propane (except $C_{11}H_{11}N$, HCN, and CH_3CN still under the calcite level) and reach denudation rates similar to those of carbonates or even gypsum. C_2H_2 and C_3H_4 would behave like carbonates (in ethane) or gypsum (in propane). C_4H_4 and C_4H_6 behave like salts in those liquids and are even more soluble than gypsum. C_4H_{10} and C_2H_4 are halite-like materials, extremely soluble in ethane and propane. Therefore, the likelihood of developing dissolution landforms in a hydrocarbon-dominated substrate, by analogy with the Earth, is high.

5.2. Present Denudation Rates on Titan Over a Titan Year

5.2.1. Net Precipitation Rates on Titan

Computing denudation rates over Titan timescales requires us to define the evolution of the net precipitation over one Titan year (1 Tyr $\simeq$ 29.5 Earth years). Titan's climate is primarily defined by a rainy warm "summer" season and a cold dry "winter" season, both spanning about 10 Earth years. Southern summers are shorter and more intense than those in the north [*Aharonson et al.*, 2009]. Precipitation occurs as sporadic and intense rainstorms during summer, when cloud formation is observed [*Roe et al.*, 2002; *Schaller et al.*, 2006, 2009; *Rodriguez et al.*, 2009, 2011; *Turtle et al.*, 2011a, 2011b].

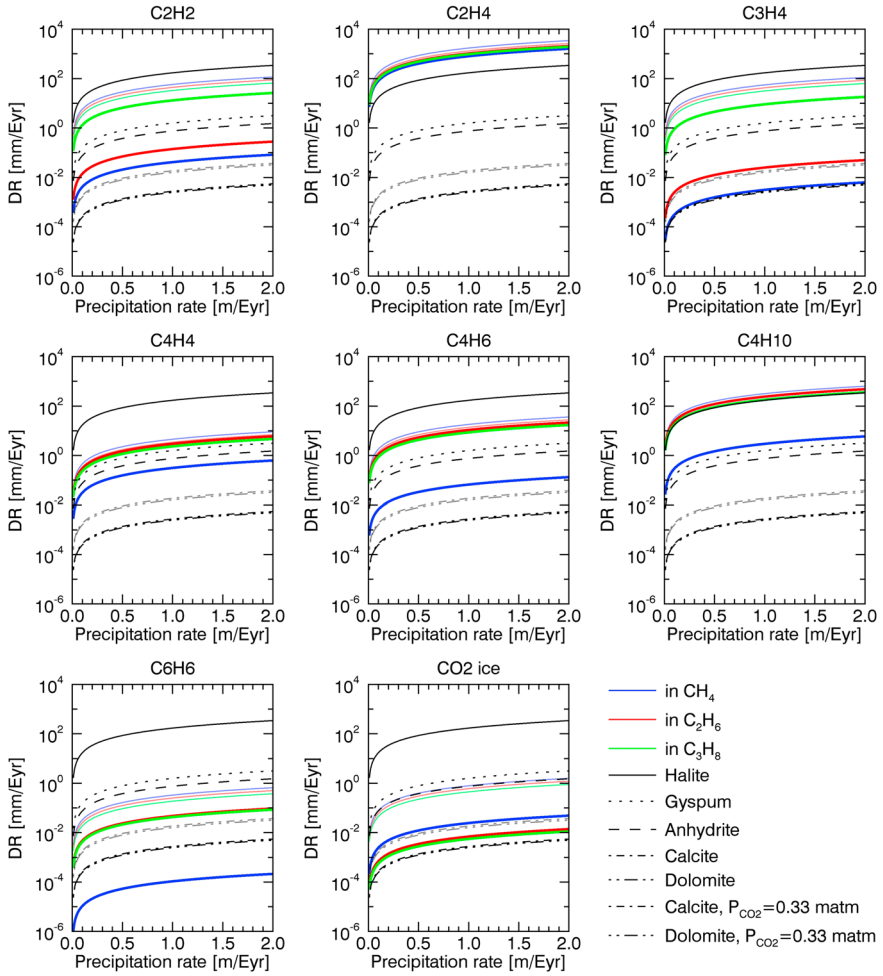

Figure 3. Denudation rates (in mm/Eyr) of nonpolar to slightly polar molecules (hydrocarbons and carbon dioxide ice) in Titan's liquids at 91.5 K (light curves: IST, bold curves: RST) compared to those of Earth's minerals in liquid water at 298.15 K (EST). The partial pressure of carbon dioxide for acid dissolution is set to 0.33 matm.

A few Global Circulation Models (GCM) attempt to describe, at least qualitatively, the methane cycle on Titan [e.g., *Rannou et al.*, 2006; *Mitchell*, 2008; *Tokano*, 2009; *Schneider et al.*, 2012]. Usually, net accumulation of rain is predicted at high latitudes >60° during summer, in agreement with the presence of lakes, whereas middle to low latitudes experience net evaporation, in agreement with the absence of lakes and the presence of deserts. Quantitatively, the model predictions are subject to debate since they depend on their physics (e.g., cloud microphysics, size of the methane reservoir, and radiative transfer scheme). Still, they remain our best estimates about Titan's climate.

During the summer season, the model of *Rannou et al.* [2006] predicts net precipitation rates of methane lower than 1 cm/Eyr at 70° latitude and up to 1 m/Eyr poleward of 70°, equivalent of a few μm to 2.7 mm/Earth day (Eday), respectively. The model of *Mitchell* [2008] predicts precipitation rates of about 2 mm/Earth day (Eday) in the polar regions and along an "Intertropical Convergence Zone" (ITCZ), nearly moving "pole to pole." The intermediate and moist models of *Mitchell et al.* [2009] predict precipitation roughly varying between 2 and 4 mm/Eday at the poles and along the ITCZ. These rates are consistent with those estimated in *Mitchell et al.* [2011] in order to reproduce the tropical storms seen in 2010 [*Turtle et al.*, 2011a] and with those estimated by the model of *Schneider et al.* [2012]. The model of *Tokano* [2009] also predicts similar precipitation rates (800 to 1600 kg/m^2 in half a Titan year, equivalent to precipitations between 3 and 6 mm/Eday).

Here we use the methane net precipitation rates extracted from the GCM of *Schneider et al.* [2012] to compute the present-day denudation rate on Titan. Figure 5 represents the mean net precipitation rates at various polar latitudes. High latitudes $>$ 80° would be quite humid ($\tau = 7 - 8$ m/Tyr). Lower latitudes would be

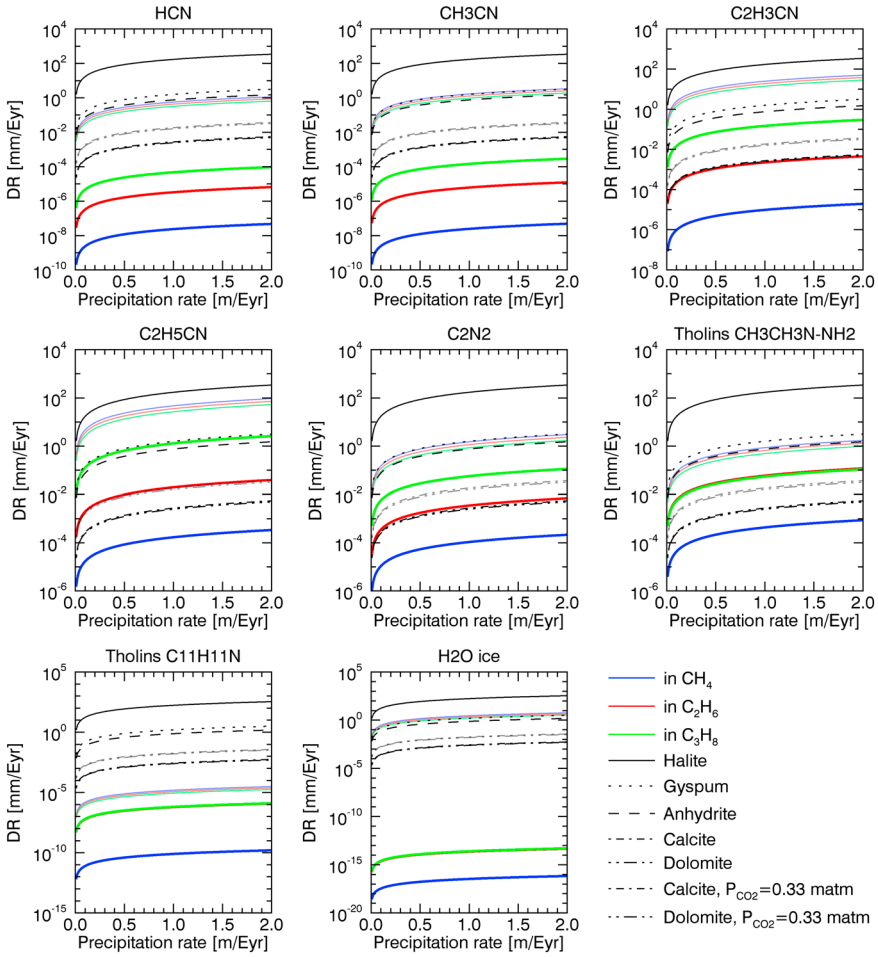

Figure 4. Same as Figure 3 but for polar molecules (nitriles and water ice).

less humid (τ=3 − 3.6 m/Tyr at 70°, decreasing to τ=0.4 − 1.6 m/Tyr at 60°). Southern low latitudes would be much drier than northern latitudes over a Titan year as a result of sparser but more intense rainstorms.

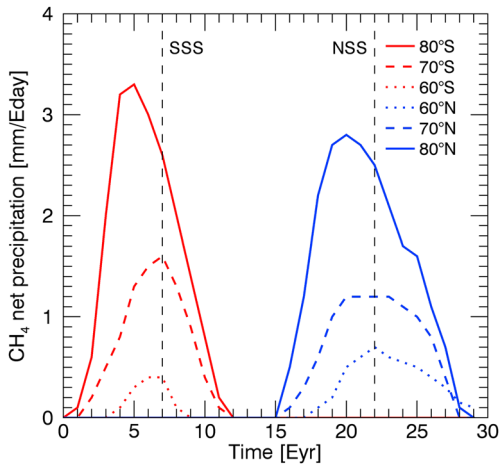

Figure 5. Net precipitation rates in mm/Earth day (Eday) at high southern and northern latitudes from *Schneider et al.* [2012] over a Titan year (29.5 Eyrs). SSS and NSS: southern and northern summer solstices.

5.2.2. Case of Pure Compounds

Figure 6 illustrates the denudation rates of a surface composed of pure organic compounds exposed to methane rains at several southern and northern polar latitudes according to the IST and RST hypotheses. Ethane and propane are not shown since the model of *Schneider et al.* [2012] only considers methane, but the behavior of Titan's solids in these liquids is already discussed in section 5.1.

Over one Titan year, the denudation rates are the highest at high latitudes and the lowest at low southern latitudes. According to the IST, all compounds would experience dissolution on the order of a few millimeters to a few meters at almost all latitudes (salt-like material), except $C_{11}H_{11}N$, the denudation rate of which would be a few hundred nanometers. The dissolution of $C_2H_8N_2$, CO_2, HCN, and C_6H_6 at 60°S, however, would be on the order of several hundred µm (carbonate-like material).

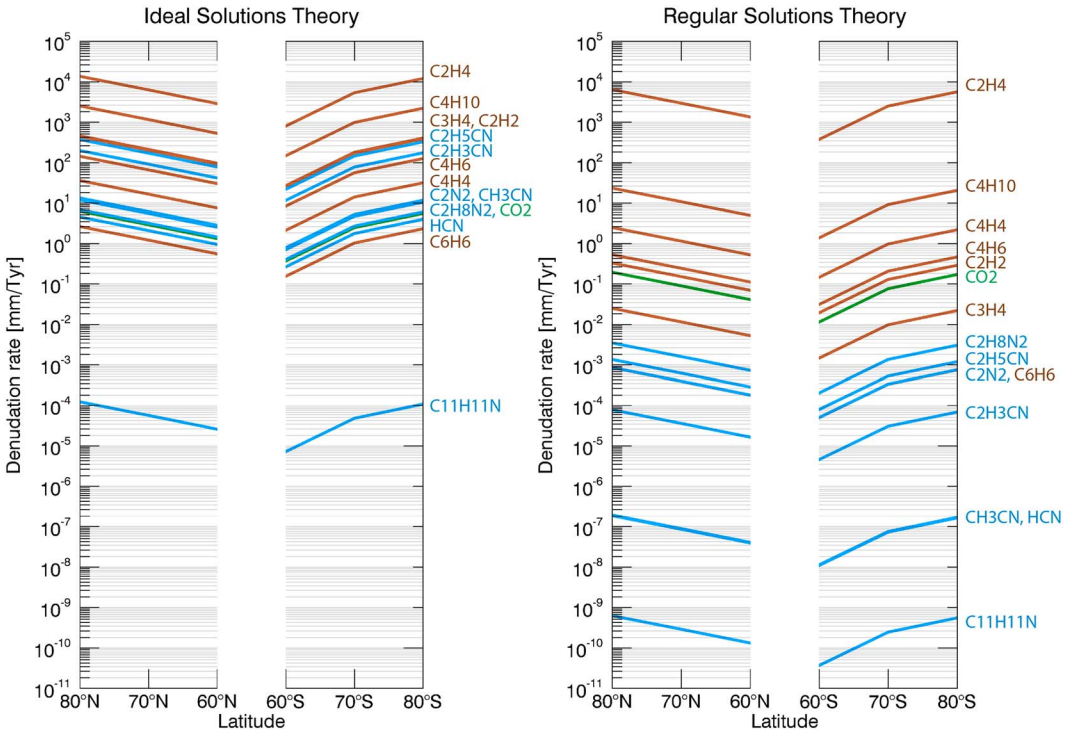

Figure 6. Denudation rates (in mm/Tyr) of Titan's surface solids in liquid methane according to the methane net precipitation rates of *Schneider et al.* [2012] over an entire Titan year for the IST and RST hypotheses. In brown are represented simple hydrocarbons, in blue the nitriles, and in green carbon dioxide.

According to the RST, C_2H_4 and C_4H_{10} denudation rates are between a few millimeters up to a few meters per Titan year (salt-like materials). The dissolution of C_4H_4, C_4H_6, C_2H_2, CO_2, and C_3H_4 is µm to hundred µm scale over a Titan year (carbonate-like materials). The denudation rates of nitriles and C_6H_6 are between 10^{-7}–10^{-10} mm/Tyr (for HCN, CH_3CN, and $C_{11}H_{11}N$) and a few µm/Tyr (carbonate to siliceous-like materials).

At high latitudes $> 70°$, we do not see much differences between the northern and the southern denudation rates, as expected from the similarities in precipitation rate between the two poles shown in Figure 5. At low southern latitudes, net precipitation rates are too low over one Titan year to allow a rapid and significant dissolution. Interestingly, Ontario Lacus and Sikun Labyrinthus, two landforms compared with terrestrial karsto-evaporitic and karstic landforms [*Malaska et al.*, 2010; *Cornet et al.*, 2012], are observed at latitudes greater than 70°S, and no other well-developed dissolution-related landforms are seen at lower southern latitudes.

Therefore, if Titan's surface is composed of pure hydrocarbons, dissolution processes are likely to occur but the formation of a karstic-like landscapes would be roughly 30 times slower on Titan than on Earth due to Titan's seasonality in precipitation. Of course, this latter consideration depends on the actual composition of the surface, which is unlikely to be pure, and of the accuracy of the climate model used.

5.2.3. Case of a Mixed Surface Layer

We now assume the presence of a surface layer, the composition of which is proportional to the accumulation rates at the surface (h_i) of solids coming from the atmosphere, calculated in the same way as *Malaska et al.* [2011] did

$$h_i = p_i V^S_{\mathrm{m,i}}/N_A \qquad \text{(m/Eyr)}, \tag{4}$$

where p_i is the production rate of molecules (in molecules/m^2/Eyr) listed in Table 1, $V^S_{\mathrm{m,i}}$ is the molar volume of the solid (or subcooled liquid if the former is not known, in m^3/mol), and N_A is the Avogadro number ($\simeq 6.022\times10^{23}$ mol^{-1}). The composition of the mixed organic layer is then determined as percentages (f_i) of each organic compound in the layer (so that $f_i = h_i/\sum_i h_i$). This method allows us to consider the volume occupied by each molecule, which is important especially for tholins because these contribute up to 20% on

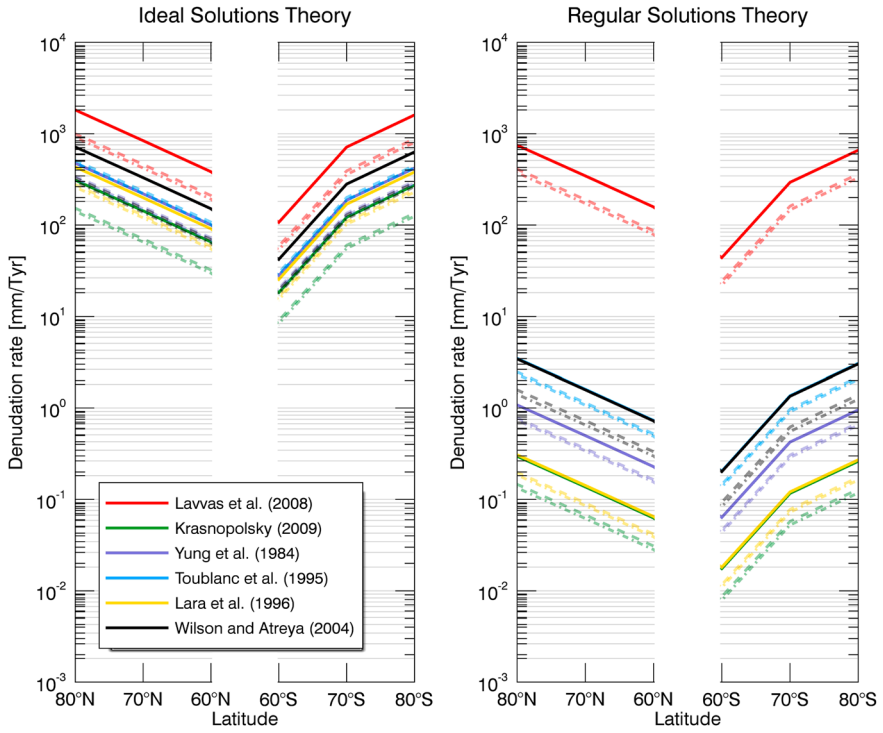

Figure 7. Denudation rates (in mm/Tyr) of Titan's surface solids in liquid methane according to the *Schneider et al.* [2012] model net precipitation rates over an entire Titan year at various latitudes and for different surface layer compositions established from photochemical models, including (dashed lines) or not (solid lines) the influence of tholins (dashed line: with $C_2N_8N_2$; dash-dotted line: with $C_{11}H_{11}N$).

average to the total production rates of molecules, but they build up to $\simeq$ 50% of the total thickness of the surface deposits due to their higher molar volumes compared to those of simple hydrocarbons or nitriles.

We consider three cases for the surface composition: without tholins and with $C_2H_8N_2$ or $C_{11}H_{11}N$ as tholins. Tholins production rate is that mentioned in *Cabane et al.* [1992]. Methane precipitation rates are those of *Schneider et al.* [2012]. The denudation rates for these mixed organic layers (DR_{mix}) are computed in a linear mixing model scheme where

$$DR_{mix} = \sum_i f_i \, DR_i \qquad \text{(m/Eyr)}. \tag{5}$$

Figure 7 gives the repartition of denudation as a function of latitude and photochemical models at the end of a Titan year. According to the IST, the denudation rate of all mixed layers would be on the order of a few centimeters to a few meters over a Titan year (salt-like layers). According to the RST, the organic layer originating from the *Lavvas et al.* [2008b] model would be the most soluble (dissolution rates of a few centimeters to a few decimeters per Titan year, salt-like layer). The organic layers originating from the other models would be more carbonate-like layers over a Titan year (dissolution rates of a few tens of μm to a few millimeters per Titan year), whether tholins are included or not. The lowest solubility of all mixed layers is reached using a *Krasnopolsky* [2009]-type composition. Over a Titan year, the likelihood of developing dissolution-related landforms is therefore nonnegligible, even if the surface is not composed of pure soluble simple solids. These mixed organic layers would behave like carbonate or salty terrestrial layers over a Titan year.

6. Discussion: How Old Are Titan's Karstic Landscapes?

Despite the strong assumptions of the method described in section 4 to infer timescales of formation of terrestrial karstic landforms (we consider only chemical erosion at equilibrium without significant climate changes over the past few MEyrs), the resulting ages are consistent with ages determined by relative or absolute chronology or constitute upper limits. Therefore, the determination of the age of the lacustrine depressions on Titan probably result in maximum timescales of development. Titan's climate is believed to have remained

Table 3. Timescales Required to Dissolve 100 m of a Surface Organic Layer (Composition Given by Photochemistry in the Atmosphere) in Liquid Methane According to the Precipitation Rates of *Schneider et al.* [2012]

	IST		RST	
Latitude	Minimum (kEyrs)	Maximum (kEyrs)	Minimum (kEyrs)	Maximum (MEyrs)
80°N	1.6	20.9	3.9	22.1
70°N	3.5	45.2	8.5	47.8
60°N	7.7	99.0	18.7	104.6
60°S	27.6	354.9	67.1	375.1
70°S	4.1	53.2	10.1	56.2
80°S	1.8	23.7	4.5	25.0

quite stable over the recent past, with a small periodic insolation variation of ± 2 W/m^2 at the poles during the last MEyr, for the current low insolation at the north pole [*Aharonson et al.*, 2009]. This probably brings some stability to the calculations.

By applying our simple model, we compute the timescales needed to form a 100 m deep depression by dissolution of a superficial mixed organic layer under the current climate conditions evaluated by *Schneider et al.* [2012]. These are shown in Table 3 and Figure 8. We compute our formation timescales using both the IST and the RST since the solubility of polar molecules is not well constrained by the RST and could get closer to that computed using the IST. However, we consider timescales evaluated using the RST as our references since they present the most conservative values for the age of the lacustrine depressions.

Independent of the thermodynamic theory considered, Titan's lacustrine depressions would be young. Among all the compositions tested, the time needed to carve a 100 m deep depression by dissolution under current climate conditions at latitudes poleward of 70° would be between a few kEyrs (IST) and 56 MEyrs (RST). At 60°N, a 100 m deep depression would be created in 7.7 kEyrs (IST) to 104.6 MEyrs (RST) while the same depression would be created in 27.6 kEyrs (IST) to 375.1 MEyrs (RST) at 60°S. This strong difference between the two hemispheres could explain why Titan's south polar regions are deprived of well-developed lacustrine depressions compared to the north.

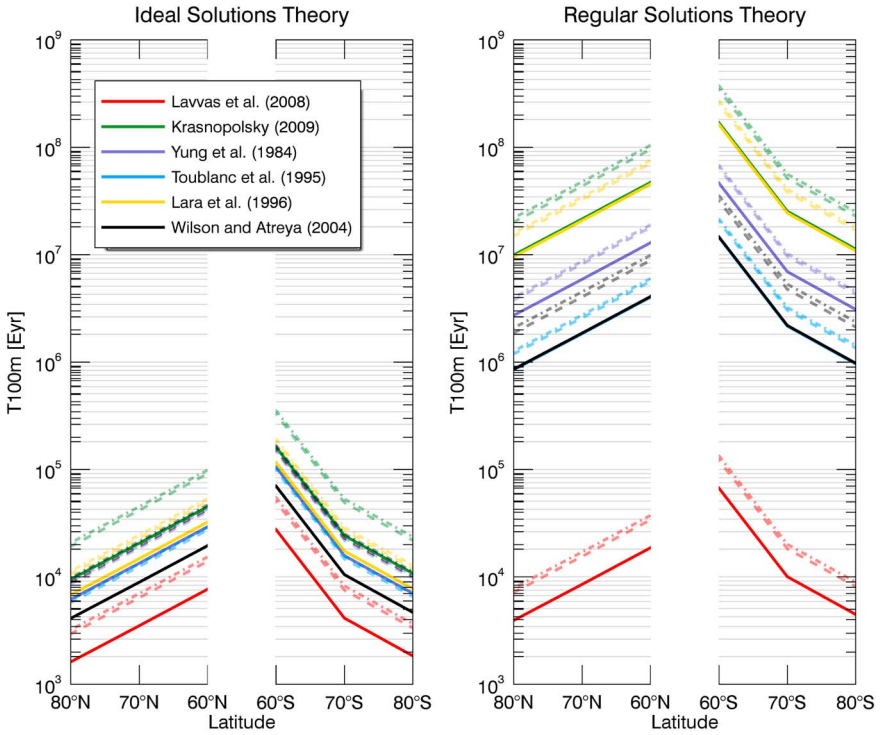

Figure 8. Same as Figure 7 but for the timescales of formation (in Eyr) of 100 m deep depressions on Titan.

It should be noted that the hypothesized timescale difference between the northern and the southern low latitudes results from an extrapolation of Titan's current climate to the past. *Aharonson et al.* [2009] showed that Croll-Milankovich-like cycle with periods of 45 (and 270) kEyrs could exist on Titan, resulting in a N-S reversal in insolation and likely subsequent climate conditions. Over geological timescales, the N-S differences in denudation rates and timescales estimated at these latitudes could be smoothed by these cycles. However, as noted earlier, we made the same extrapolation for the Earth, whose climate dramatically changed over time, without obtaining unreasonable formation timescales.

In any case, all these timescales are consistent with the youth of Titan's surface as determined from (1) crater counting (0.3–1.2 GEyrs, *Neish and Lorenz* [2012]), (2) dune sediment inventory (50–730 MEyrs, *Sotin et al.* [2012] and *Rodriguez et al.* [2014]), (3) the flattening of the poles due to the substitution of methane by ethane in clathrates (500 MEyrs if restricted to the poles or 0.3–1.7 GEyrs if not, *Choukroun and Sotin*) [2012], and the possible methane outgassing event (1.7–2.7 GEyrs, *Tobie et al.* [2006]).

In summary, the morphology of Titan's lacustrine depressions suggests that dissolution occurs on Titan. The denudation rates of pure organic compounds and a mixed organic layer as compared to those of soluble minerals on Earth also supports this hypothesis. The timescales needed to dissolve various amounts of material as compared to the timescales of development of karstic landforms on Earth are also quite consistent in the sense that karstic landscapes are usually relatively young landscapes. Finally, the latitudinal repartition of denudation rates and timescales of dissolution is consistent with the latitudinal repartition of the possible dissolution-related landforms at the surface of Titan. The surface dissolution scenario for the origin of Titan's lakes appears very likely and Titan's lakes could be among the youngest features of the moon.

7. Conclusion

Titan's lakes result from the filling of topographic depressions by surface or subsurface liquids. Their morphology led to analogies with terrestrial landforms of various origins (volcanic, thermokarstic, karstic, evaporitic, or karsto-evaporitic). The karstic/karsto-evaporitic dissolution scenario seems to be the most relevant, given the nature of surface materials on Titan and its climate. We constrained the timescales needed for the formation of Titan's depressions by dissolution, on the basis of the current knowledge on the development of terrestrial karsts.

We computed solutional denudation rates from the theory developed by *White* [1984]. This simple theory needs three parameters: the solubilities and the densities of solids and liquids at a given temperature and a climatic parameter linked to the net precipitation rates onto the surface. We computed the solubilities of terrestrial minerals in liquid water at 25°C and tested the model by computing the denudation rates and timescales of formation of several terrestrial examples of karstic landforms.

We then applied the same model to Titan. We computed the solubilities of Titan's surface organic compounds in pure liquid methane, ethane, and propane at 91.5 K using different thermodynamic theories. We evaluated the molar volumes of liquid and solid Titan's surface compounds at 91.5 K, and we used the results of the recent GCM of *Schneider et al.* [2012] as input for the precipitation rates of methane on Titan, which allowed us to compute denudation rates at several latitudes. Denudation rates have then been computed for pure organic compounds at Earth and Titan timescales and have been compared to those determined for soluble minerals on Earth. We also computed denudation rates for three different compositions of the surface organic layer. Over one Titan year, these mixed layers of organic compounds behave like terrestrial salts or carbonates, which indicates their high susceptibility to dissolution, though these processes would be 30 times slower on Titan than on Earth due to the seasonality (rainfall occurs only during Titan's summer).

We computed theoretical timescales for the formation of 100 m deep depressions in mixed organic layers under present climatic conditions. As with dissolution landforms on Earth, Titan's depressions would be young. At high polar latitudes, we found that the timescales of development for depressions are relatively short (on the order of 50 MEyrs at maximum to carve 100 m) and consistent with the young age of Titan's surface. These timescales are consistent with the existence of numerous lacustrine depressions and dissected landscapes at these latitudes. At southern low latitudes, the computed timescales are as long as 375 MEyrs due to the low precipitation rates. This low propensity to develop depressions by dissolution is consistent with their relative absence/bare formation at low latitudes. Over geological timescales greater than those of Titan's

Croll-Milankovitch cycles (45 and 270 kEyrs), this difference would probably be strongly attenuated. However, climate model predictions are not presently available over geologic timescales, and the present-day seasonal climate variations are the best that can be currently constrained.

The results of these simple calculations are consistent with the hypothesis that Titan's depressions most likely originate from surface dissolution. Theoretical timescales for the formation of these landforms are consistent with the other age estimates of Titan's surface. Future works could include the effects of rain in equilibrium with the nitrogen, ethane, and propane atmospheric gases in the raindrop composition (e.g., *Graves et al.* [2008] or *Glein and Shock* [2013]). Experimental constraints on the solubility of gases and solids in liquids thanks to recent technical developments for Titan experiments [*Luspay-Kuti et al.*, 2012, 2014; *Malaska and Hodyss*, 2014; *Chevrier et al.*, 2014; *Leitner et al.*, 2014; *Singh et al.*, 2014] would also be of extreme importance for such work. Finally, the influence of other landshaping mechanisms such as collapse or subsurface fluid flows, which play a significant role in the development of some karstic landforms on Earth, could also be implemented.

Appendix A: List of Compound Names for Titan

CH_4: methane (liquid)
C_2H_6: ethane (liquid)
C_3H_8: propane (liquid)
C_4H_{10}: n-butane
C_2H_2: acetylene
C_2H_4: ethylene
C_3H_4: methyl-acetylene
C_4H_4: vinyl-acetylene
C_4H_6: 1-3 butadiene
C_6H_6: benzene
HCN: hydrogen cyanide
C_2N_2: cyanogen
CH_3CN: acetonitrile
C_2H_3CN: acrylonitrile
C_2H_5CN: propionitrile
$C_2H_8N_2$: 1-1 dimethyl-hydrazine (tholins-like)
$C_{11}H_{11}N$: quinoline (tholins-like)
H_2O: water ice Ih
CO_2: carbon dioxide ice

Appendix B: Solubility of Solids on Earth and Titan

B1. Dissolution Processes on Earth

Dissolution occurs in karstic to evaporitic areas on Earth, where the dominant minerals are calcite, dolomite, halite, anhydrite, or gypsum. Basic aqueous reactions of congruent dissolution for these common soluble minerals (i.e., all components of the minerals dissolve entirely) are summarized below:

$$CaCO_3 + H_2O + CO_2 \iff Ca^{2+} + 2HCO_3^-$$
$$CaMg(CO_3)_2 + 2H_2O + 2CO_2 \iff Ca^{2+} + Mg^{2+} + 4HCO_3^-$$
$$CaSO_4.2H_2O \iff Ca^{2+} + SO_4^{2-} + 2H_2O$$
$$CaSO_4 + H_2O \iff Ca^{2+} + SO_4^{2-} + H_2O$$
$$NaCl + H_2O \iff Na^+ + Cl^- + H_2O.$$

Halite (NaCl), gypsum ($CaSO_4.2H_2O$), and anhydrite ($CaSO_4$) dissolve by pure dissociation, and calcite ($CaCO_3$) and dolomite ($CaMg(CO_3)_2$) dissolve by dissociation and acid dissolution, i.e., with the help of the CO_2 gas dissolved in water [*Langmuir*, 1997; *Ford and Williams*, 2007; *Brezonik and Arnold*, 2011].

Table B1. Thermodynamic and Physical Parameters of Minerals, Water, and Ions Considered in the Dissolution Reactions, Collected From the Literature [*Lide*, 2010; *Langmuir*, 1997; *Ford and Williams*, 2007; *Brezonik and Arnold*, 2011; *White*, 2013]

Name	Formula	M_i (g/mol)	z_i	a_i (Å)	b_i (kg/mol)	$\Delta_f G_i^\circ$ (kJ/mol)	$\Delta_f H_i^\circ$ (kJ/mol)
			Minerals				
Calcite	$CaCO_3$	100.087	0	-	-	−1129.1	−1207.6
Dolomite	$CaMg(CO_3)_2$	184.401	0	-	-	−2161.7	−2324.5
Gypsum	$CaSO_4.2H_2O$	172.171	0	-	-	−1797.2	−2022.6
Anhydrite	$CaSO_4$	136.141	0	-	-	−1321.7	−1434.1
Halite	NaCl	58.443	0	-	-	−384.1	−411.2
			Aqueous Species				
Chlore	Cl^-	35.460	−1	3.71	0.01	−131.3	−167.2
Sodium	Na^+	22.990	+1	4.32	0.06	−261.9	−240.1
Hydroxyl	OH^-	17.007	−1	10.65	0.21	−157.3	−230
Hydrogen	H^+	1.008	+1	4.78	0.24	0	0
Calcium	Ca^{2+}	40.080	+2	4.86	0.15	−553.54	−542.83
Magnesium	Mg^{2+}	24.320	+2	5.46	0.22	−454.8	−466.8
Sulfate	SO_4^{2-}	96.060	−2	5	−0.04	−744.6	−909.2
Carbonate	CO_3^{2-}	60.010	−2	5.4	0	−527.9	−677.1
Bicarbonate	$HCO3^-$	61.020	−1	5.4	0	−586.8	−692
Carbonic acid	H_2CO_3	62.025	0	-	-	−623.2	-699.7
			Solvent and Gas				
Water	H_2O	18.015	0	-	-	−237.18	−285.83
Carbon dioxide	CO_2	44.010	0	-	-	−394.4	−393.51

The physical and thermodynamic parameters needed to compute solubilities are given in Table B1. Ideal and nonideal electrolyte theories are considered. We also consider the acid dissolution of carbonate minerals.

B1.1. Pure Dissociation of Minerals: Halite, Anhydrite and Gypsum

For a given chemical reaction implying A and B and producing C and D, with their respective stoichiometric numbers a, b, c, and d, the law of mass action gives

$$aA + bB \iff cC + dD, \tag{B1}$$

where one can define a thermodynamical equilibrium constant (or thermodynamic solubility product) for the reaction K_{eq} (often written pK_{eq}, with $pK_{eq} = -\log K_{eq}$), so that

$$K_{eq} = \frac{(C)^c\,(D)^d}{(A)^a\,(B)^b} = \frac{(m_C\Gamma_C)^c\,(m_D\Gamma_D)^d}{(m_A\Gamma_A)^a\,(m_B\Gamma_B)^b}, \tag{B2}$$

where (i) denotes the activity of the ith compound, being the product of an activity coefficient Γ_i and a molality m_i (in mol/kg of solvent). For liquids and solids reacting together (or being produced) during a congruent dissolution reaction, the activity is set to unity. The equilibrium constant can be derived from thermodynamics at standard state ($T = 25°C$ and $P = 1$ atm) using the Gibbs-Helmholtz equation:

$$\Delta_r G^\circ = -R\,T\,\ln K_{eq} = -2.303\,R\,T\,\log K_{eq} \qquad \text{(J/mol)}, \tag{B3}$$

where $\Delta_r G^\circ$ is the standard Gibbs free energy of reaction (in J/mol), calculated using the Hess' law:

$$\Delta_r G^\circ = \sum_{\text{products}} n_i\,\Delta_f G_i^\circ - \sum_{\text{reactants}} n_j\,\Delta_f G_j^\circ \qquad \text{(J/mol)}, \tag{B4}$$

with $\Delta_f G^\circ$ being the standard Gibbs free energy of formation of each species (in J/mol) and n their stoichiometric numbers. Following the same principle, we compute the standard enthalpy of reaction $\Delta_r H^\circ$ (J/mol) from the individual enthalpies of formation $\Delta_f H^\circ$ (in J/mol). The standard enthalpy of reaction is then used to

Journal of Geophysical Research: Planets

10.1002/2014JE004738

Table B2. Thermodynamic Constants of Dissociation and Dissolution Reactions in Standard Conditions (at 25° C and 1 atm)

Reaction	Equations	$\Delta_r G°$ (kJ/mol)	$\Delta_r H°$ (kJ/mol)	K_{eq}	pK_{eq}	Equilibrium Constant Expression
	Pure Dissociation Reactions for Minerals					
Gypsum dissociation	$CaSO_4.2H_2O \iff Ca^{2+} + SO_4^{2-} + 2H_2O$	24.70	−1.09	4.71×10^{-5}	4.327	$K_{gd} = (Ca^{2+})(SO_4^{2-})$
Anhydrite dissociation	$CaSO_4 \iff Ca^{2+} + SO_4^{2-}$	23.56	−17.93	7.46×10^{-5}	4.128	$K_{ad} = (Ca^{2+})(SO_4^{2-})$
Halite dissociation	$NaCl \iff Na^{+} + Cl^{-}$	−9.10	3.90	39.29	−1.594	$K_{hd} = (Na^{+})(Cl^{-})$
Calcite dissociation	$CaCO_3 \iff Ca^{2+} + CO_3^{2-}$	47.36	−12.53	5.05×10^{-9}	8.297	$K_{cd} = (Ca^{2+})(CO_3^{2-})$
Dolomite dissociation	$CaMg(CO_3)_2 \iff Ca^{2+} + Mg^{2+} + 2CO_3^{2-}$	97.56	−39.33	8.10×10^{-18}	17.092	$K_{dd} = (Ca^{2+})(Mg^{2+})(CO_3^{2-})^2$
	Secondary Dissociation Reactions and Dissolution Reactions for Carbonates Dissolution					
CO_2 dissolution	$CO_2 + H_2O \iff H_2CO_3^{\circ}$	8.38	−20.36	3.40×10^{-2}	1.468	$K_{CO_2} = (H_2CO_3^{\circ})/P_{CO_2}$
Carbonic acid dissociation	$H_2CO_3^{\circ} \iff H^{+} + HCO_3^{-}$	36.40	7.70	4.20×10^{-7}	6.377	$K_1 = (H^{+})(HCO_3^{-})/(H_2CO_3^{\circ})$
Bicarbonate dissociation	$H^{+} + CO_3^{2-} \iff HCO_3^{-}$	58.90	14.90	4.80×10^{-11}	10.319	$K_2 = (HCO_3^{-})/(H^{+})(CO_3^{2-})$
Calcite dissolution	$CaCO_3 + H_2O + CO_2 \iff Ca^{2+} + 2\,HCO_3^{-}$	33.24	−40.09	1.50×10^{-6}	5.823	$K_{cal} = (Ca^{2+})(HCO_3^{-})^2/P_{CO_2}$
Dolomite dissolution	$CaMg(CO_3)_2 + 2H_2O + 2CO_2 \iff Ca^{2+} + Mg^{2+} + 4\,HCO_3^{-}$	69.32	−94.45	7.17×10^{-13}	12.144	$K_{dol} = (Ca^{2+})(Mg^{2+})(HCO_3^{-})^4/P_{CO_2}^2$

Table B3. Molalities (in mol/kg of Solvent) of Minerals in Water at 25°C According to the Ideal and the Electrolyte Solutions Theories[a]

Name	IST	EST
	Dissolution by Dissociation	
Halite	6.27	6.27
Gyspum	8.63×10^{-3}	2.26×10^{-2}
Anhydrite	6.86×10^{-3}	1.62×10^{-2}
Calcite	7.10×10^{-5}	7.72×10^{-5}
Dolomite	3.77×10^{-5}	4.11×10^{-5}
	Acid Dissolution	
Calcite, $P_{CO_2} = 0.33$ matm	4.99×10^{-4}	5.42×10^{-4}
Dolomite, $P_{CO_2} = 0.33$ matm	2.59×10^{-4}	2.76×10^{-4}
Calcite, $P_{CO_2} = 0.01$ atm	1.55×10^{-3}	1.80×10^{-3}
Dolomite, $P_{CO_2} = 0.01$ atm	8.09×10^{-4}	8.99×10^{-4}
Calcite, $P_{CO_2} = 0.11$ atm	3.46×10^{-3}	4.28×10^{-3}
Dolomite, $P_{CO_2} = 0.11$ atm	1.80×10^{-3}	2.09×10^{-3}

[a] $P_{CO_2} = 0.33$ matm refers to normal dry air [*Langmuir*, 1997] while $P_{CO_2} = 0.01$ atm more refers to tropical climate environments [*Fleurant et al.*, 2008], which actually could even reach considerable CO_2 content in the soils of up to $P_{CO_2} = 0.11$ atm [*Ford and Williams*, 2007].

compute the equilibrium constants at temperatures that differ from standard conditions using the Van't Hoff equation [*Langmuir*, 1997] as follows:

$$\ln \frac{K_{T2}}{K_{T1}} = \frac{\Delta_r H_i^o}{R} \left(\frac{1}{T_1} - \frac{1}{T_2} \right), \qquad \text{(B5)}$$

where K_{T1} and K_{T2} are the equilibrium constant of a given chemical reaction at two different temperatures T_1 and T_2 (in K) (the subscript 1 is used to indicate the reference state, 25°C in this case). Table B2 gathers the thermodynamic parameters for all the considered dissolution reactions. It also displays each equilibrium constant equation for common terrestrial minerals.

B1.2. Acid Dissolution of Carbonates: Calcite and Dolomite

For calcium and magnesium carbonates, a set of reactions happens, not only involving the mineral dissociation itself (K_{cd} or K_{dd}) but also including the carbon dioxide gas dissolution in water (K_{CO_2}), which produces carbonic acid that acidifies water. Then, carbonic acid rapidly dissociates into bicarbonate ions (K_1), which are also created by the association of protons H^+ and carbonate ions (K_2). The thermodynamic properties of these intermediate reactions to the dissolution of calcite and dolomite are summarized in Table B2. The activity of carbon dioxide is approximately equal to its partial pressure (P_{CO_2}, see *Langmuir* [1997] and *Ford and Williams* [2007]) so that, for calcite acid dissolution, one can write

$$K_{cal} = \frac{(Ca^{2+})\,(HCO_3^-)^2}{P_{CO_2}} = \frac{K_1\, K_{CO_2}\, K_{cd}}{K_2}, \qquad \text{(B6)}$$

and for dolomite acid dissolution:

$$K_{dol} = \frac{(Ca^{2+})\,(Mg^{2+})\,(HCO_3^-)^4}{P_{CO_2}^2} = \frac{K_1^2\, K_{CO_2}^2\, K_{dd}}{K_2^2}. \qquad \text{(B7)}$$

Assuming a given partial pressure of carbon dioxide, one can compute the activity, molality, and mole fraction at saturation of calcite and dolomite in water. The molality of CO_2 in the system is calculated thanks to the Henry law ($m_{CO_2} = k_H(T)\, P_{CO_2}$, $K_H(T)$ being Henry's law constant, varying with temperature). We performed the calculations for three values of P_{CO_2} at 25°C: $P_{CO_2} = 0.33$ matm, which represents the normal dry air [*Langmuir*, 1997] that could be quite analogous to atmospheric conditions in arid/semiarid areas, and $P_{CO_2} = 0.01$–0.11 atm, which represents values encountered in more humid areas such as under equatorial/tropical climates [*Ford and Williams*, 2007; *Fleurant et al.*, 2008].

B1.3. Activity Coefficients for Electrolyte Solutions

We infer the molalities m_i and activities (i) of ions in solution from K_{eq} at different temperatures under an Ideal (IST, $\Gamma_i = 1$) and a nonideal Electrolyte (EST, $\Gamma_i \neq 1$) Solution Theory. For the EST, the activity coefficients Γ_i are calculated by iteration using the extended Debye-Hückel equation as modified by *Truesdell and Jones* [1974]:

$$\log \Gamma_i = -A\, z_i^2 \left(\frac{\sqrt{I}}{1 + B\, a_i \sqrt{I}} \right) + b_i\, I, \qquad \text{(B8)}$$

where I is the molal ionic strength of the solution, defined as follows:

$$I = \frac{1}{2} \sum_{i=1}^{n} m_i\, z_i^2 \qquad \text{(mol/kg)}, \qquad \text{(B9)}$$

Table B4. Melting and Boiling Points Thermodynamic Constants of Titanian Materials[a]

Formula	T_m (K)	$\Delta_m H°$ (kJ/mol)	T_b (K)	$\Delta_v H°$ (kJ/mol)
CH_4	90.680	0.940	111.670	8.190
C_2H_6	90.360	0.582	184.570	14.690
C_3H_8	85.460	3.500	232.040	19.040
C_4H_{10}	134.850	4.660	272.660	22.440
C_2H_2	192.450	4.105	188.450	16.674
C_2H_4	104.000	3.350	169.380	13.530
C_3H_4	170.450	5.349	249.950	22.185
C_4H_4	227.600	7.687	278.250	22.470
C_4H_6	164.240	7.980	268.740	22.470
C_6H_6	278.640	9.870	353.240	30.720
HCN	259.860	8.406	298.850	26.896
C_2N_2	245.320	8.110	252.100	23.330
CH_3CN	229.330	8.160	354.800	29.750
C_2H_3CN	189.670	6.230	350.450	32.600
C_2H_5CN	207.150	5.030	350.500	31.810
$C_2H_8N_2$	215.950	10.070	337.050	28.477
$C_{11}H_{11}N$	326.650	20.418	538.855	50.005
H_2O	273.150	6.010	373.200	40.650
CO_2	216.592	9.020	194.600	15.326

[a]Data gathered from *Lide* [2010] and *Yaws* [1996]. The melting properties of $C_{11}H_{11}N$ have been taken in *Chirico et al.* [2007].

where z_i is the charge of i and a_i and b_i are the two parameters of the *Truesdell and Jones* [1974] equation (a modified hydrated radius, in Å, and a purely empirical parameter, respectively). A and B are two variables depending on the temperature T (in °C), defined as follows [*Ford and Williams*, 2007]:

$$A = 0.4883 + 8.074 \times 10^{-4}\, T \qquad \text{(B10)}$$

$$B = 0.3241 + 1.6 \times 10^{-4}\, T. \qquad \text{(B11)}$$

Results from these calculations are given in Table B3. The calculation of activity coefficients has a relatively minor impact in the change of molality for carbonates, while a clear difference can be seen for salts (anhydrite and gypsum). The presence of CO_2 in the carbonate-water system greatly increases the amount of dissolved carbonates, until reaching solubilities roughly similar to those of gypsum and anhydrite. The EST molalities has been used for all minerals except for halite, which possesses a ionic strength too strong to be computed using our Debye-Hückel equation.

B2. Solubility of Titan's Solids

The solubility of Titan's solids in pure liquid hydrocarbons is calculated according to the Van't Hoff equation:

$$\ln \Gamma_i X_{i,\text{sat}} = \frac{\Delta_m H_i^\circ}{R}\left(\frac{1}{T_{m,i}} - \frac{1}{T}\right), \qquad \text{(B12)}$$

where Γ_i is the activity coefficient of the solute, $X_{i,\text{sat}}$ its mole fraction at saturation, $\Delta_m H_i^\circ$ its enthalpy of melting (in J/mol) evaluated at $T_{m,i}$, its melting temperature (in K), which differs from the temperature of the solution T (K), and R is the ideal gas constant. Melting properties of Titan compounds are given in Table B4.

We consider the case of the Ideal Solutions Theory (IST), for which $X_{i,\text{sat}}$ is calculated by assuming $\Gamma_i = 1$ (all the molecules share the same affinity with each other), and the case of the Regular Solutions Theory (RST) of *Preston and Prausnitz* [1970] for which $\Gamma_i \neq 1$ (molecules have preferential affinity with one or the other). The latter approach has already been used in several publications dealing with the lakes and seas composition [*Raulin*, 1987; *Dubouloz et al.*, 1989; *Cordier et al.*, 2009, 2013b].

The RST requires to compute Γ_i's. Assuming the subscripts 1 for the solvent and 2 for the solute, the RST gives

$$\ln \Gamma_2 = \frac{(\delta_1 - \delta_2)^2 + 2\, l_{12}\delta_1\delta_2}{R\,T}\, V_{m,2}^L\, \phi_1^2, \qquad \text{(B13)}$$

where $V_{m,2}^L$ is the subcooled liquid molar volume of the solute (in m^3/mol), l_{12} is the empirical interaction parameter between the solvent and the solute taken from various sources (e.g. *Preston and Prausnitz* [1970] and *Szczepaniec-Cieciak et al.* [1978]), ϕ_1 is the volume fraction of the liquid, computed as follows:

$$\phi_1 = \frac{(1 - X_2)\, V_{m,1}^L}{(1 - X_2)\, V_{m,1}^L + X_2\, V_{m,2}^L}, \qquad \text{(B14)}$$

and δ_1 and δ_2 are the Hildebrand solubility parameters of the solvent and the solute, respectively, (in $(J/m^3)^{1/2}$ computed from their enthalpy of vaporization $\Delta_v H_i$ (J/mol), as follows:

$$\delta_i^2 = \frac{\Delta_v H_i - R\,T}{V_{m,i}^L} \qquad ((J/m^3)^{1/2}), \qquad \text{(B15)}$$

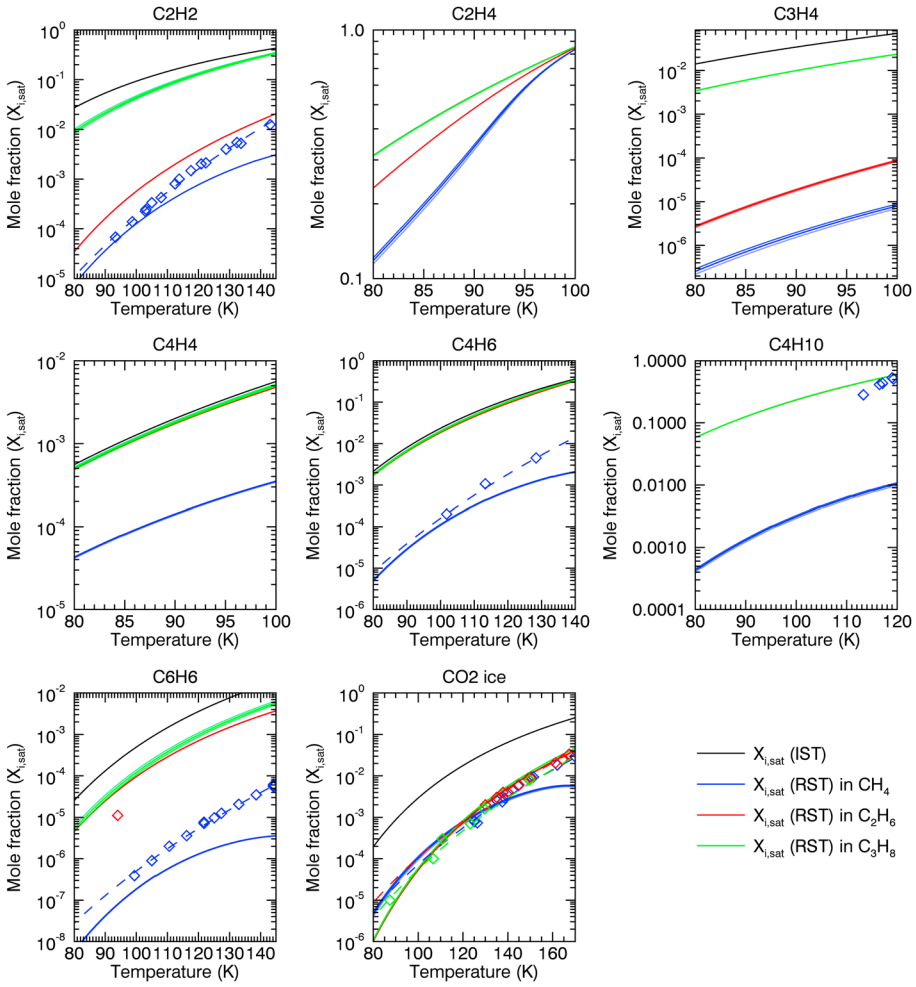

Figure B1. Saturation mole fraction of Titan's "nonpolar solids" (hydrocarbons and carbon dioxide ice) in Titan's liquids computed using the RST and IST, and different Rackett equations (see section C1). The darkest curves represent $X_{i,\mathrm{sat}}$ evaluated by equation (C3) with the Z_{RA} parameter. Diamonds are experimental values collected for C_4H_{10} [*Brew*, 1977; *Kuebler and McKinley*, 1975], C_2H_2 [*Neumann and Mann*, 1969], C_4H_6 [*Preston et al.*, 1971], C_6H_6 [*von Szalghary*, 1972; *Luks et al.*, 1981; *Kuebler and McKinley*, 1995; *Malaska and Hodyss*, 2014], and CO_2 [*Clark and Din*, 1953; *Davis et al.*, 1962; *Cheung and Zander*, 1968; *Preston et al.*, 1971] in the corresponding liquids. Dashed lines are empirical power fits of the experimental points (with $R^2 > 0.98$).

where $\Delta_v H_i$ is taken in the literature at the boiling point temperature T_b (Table B4) for each compound and extrapolated down to lower temperatures using the Watson equation [*Poling et al.*, 2007]:

$$\Delta_v H_{i,T} = \Delta_v H_{i,Tb} \left(\frac{1 - T/T_c}{1 - T_b/T_c} \right)^{0.38} \quad \text{(J/mol)}. \tag{B16}$$

The solubilities are given for a wide range of temperatures in Figures B1 (nonpolar molecules) and B2 (polar molecules), on top of which we also reported experimental data points gathered from the literature, fitted by an empirical power law ($R^2 > 0.98$) in order to extrapolate the experimental values at low temperatures for comparison.

The IST hypothesis provides a first estimate of the solubility, as seen in Figures B1 and B2. It does not consider the different behavior of the solutes in the different solvents but presents the advantage of not depending on approximate calculations of the activity coefficients of each species. According to this theory, all simple hydrocarbons would thus be rather solubles at low temperatures, the least soluble being nitriles and C_6H_6.

The RST hypothesis provides a second estimate and shows that solids are less soluble in methane than in ethane and propane. Whatever the liquid, simple nitriles generally show an increase in solubility with a higher

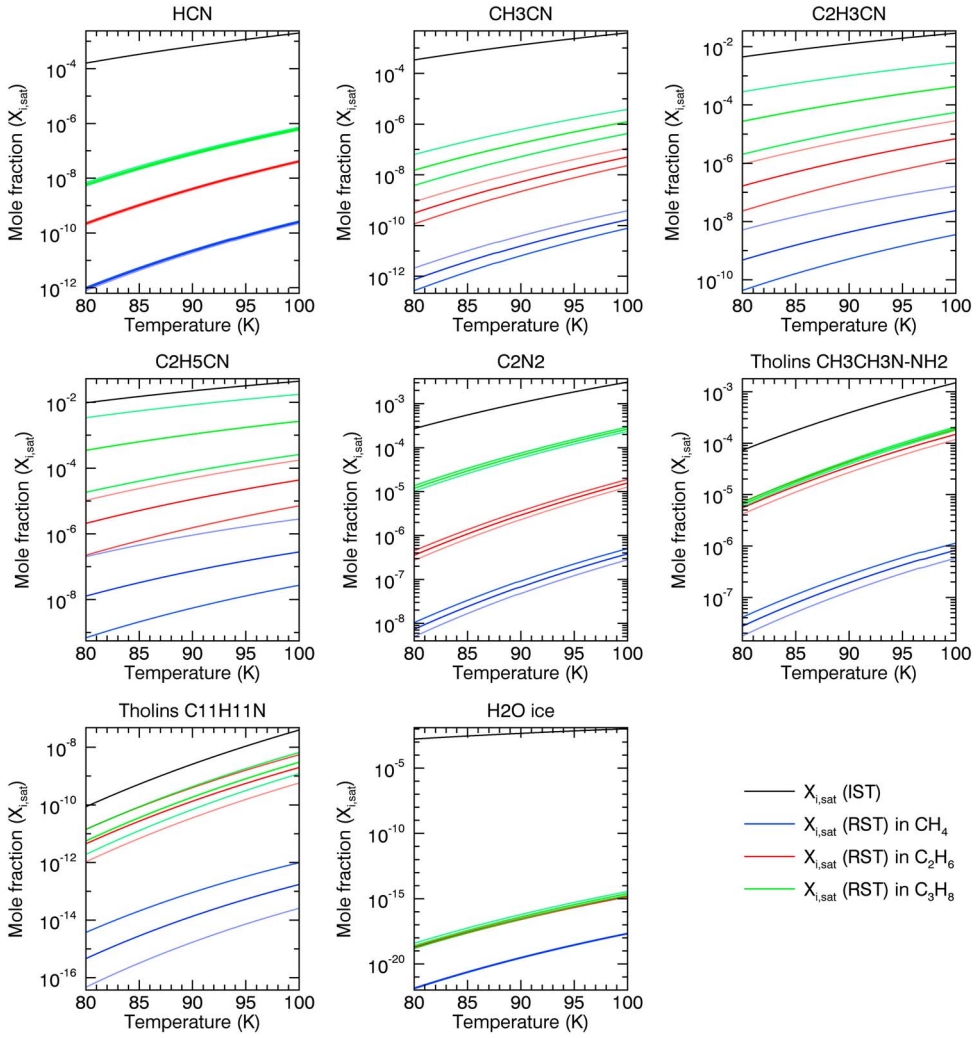

Figure B2. Same as Figure B1 but for Titan's polar solids (nitriles and water ice).

number of C atoms in their carbon chain. C_2H_4, C_4H_{10}, and C_2H_2 are the most soluble compounds again, joined by C_4H_4, C_4H_6, CO_2, C_3H_4, and finally C_6H_6. Nitriles are the least soluble compounds. At cryogenic temperatures (<100 K), the simulated solubilities are in good agreement with the power fits of experimental data (with the exception of n-butane, which shows a higher solubility in experiments). It is also worth noting that recent solubility experiments of benzene in liquid ethane have been performed at 94 K by *Malaska and Hodyss* [2014]. The $X_{i,\mathrm{sat}}$ for benzene in ethane they determined experimentally ($1.11 \pm 0.09 \times 10^{-5}$) is also quite close to our theoretical value computed using the RST at 94 K (4.42×10^{-5}), though slightly lower. This difference is probably due to the dissolution of nitrogen into liquid ethane during the experiment, which tends to lower the solubility of benzene. Benzene also reached saturation so quickly in liquid ethane (in less than 2 h) [*Malaska and Hodyss*, 2014], compared to the timescales considered in the present work, that dissolution can be assumed instantaneous. Finally, as expected, the solubility of water ice is unconstrained given the considerable range between IST and RST estimates (about a factor of 10^{17}) but is probably low.

Solubilities calculated using the IST and RST are also given at 91.5 K in Table B5 along with those gathered from our empirical fits of experimental data and the literature. The fits of experimental data are quite consistent with our RST values. Previous studies document the solubility of pure solids in liquid mixtures in equilibrium with the atmosphere (thus composed of methane, ethane, propane, and/or nitrogen) at various temperatures. Direct comparisons are therefore tentative, since the liquid composition, temperatures, and the thermodynamic parameters sources are heterogeneous. Nitrogen tends to decrease the solubility of solids in liquids while ethane and propane tend to increase it. It should be noted that the solubility of hydrocarbons is quite

Journal of Geophysical Research: Planets

10.1002/2014JE004738

Table B5. Saturation Mole Fractions of Titan's Solids in Pure Liquid Methane, Ethane, and Propane at 91.5 K Evaluated Using the Ideal Solutions and Regular Solutions Theories Compared With Our Fits at 91.5 K of Experimental Data and With Values Taken From the Literature[a]

	X_i (IST)		X_i (RST)		Experiments	R87 (RST)		D89 (RST)	C13 (IST)	G13 (MVL)	T13 (PC-SAFT)	
Formula	91.5 K		91.5 K		91.5 K	94 K		92.5 K	90 K	90.7 K	90 K	93.7 K
CH_4	-	1.00	-	-	1.00	8.60×10^{-1}	-	7.30×10^{-2}	-	6.81×10^{-1}	6.84×10^{-1}	3.18×10^{-1}
C_2H_6	-	-	1.00	-	-	-	9.70×10^{-1}	9.09×10^{-1}	-	1.55×10^{-1}	8.30×10^{-2}	5.32×10^{-1}
C_3H_8	-	-	-	1.00	-	-	-		-	1.55×10^{-2}	7.80×10^{-3}	7.20×10^{-2}
N_2	-	-	-	-	-	1.40×10^{-1}	3.00×10^{-2}	1.80×10^{-2}	-	1.48×10^{-1}	2.21×10^{-1}	6.89×10^{-2}
C_4H_{10}	1.40×10^{-1}	1.51×10^{-3}	1.39×10^{-1}	1.40×10^{-1}	-	-	-	-	1.22×10^{-1}	-	-	-
C_2H_2	5.90×10^{-2}	4.48×10^{-5}	2.00×10^{-4}	2.45×10^{-2}	5.72×10^{-5}	1.81×10^{-4}	6.93×10^{-4}	4.10×10^{-4}	5.40×10^{-2}	2.20×10^{-4}	3.40×10^{-3}	7.70×10^{-3}
C_2H_4	5.89×10^{-1}	4.02×10^{-1}	5.33×10^{-1}	5.88×10^{-1}	-	1.81×10^{-3}	4.62×10^{-2}	-	-	-	-	-
C_3H_4	3.85×10^{-2}	2.25×10^{-6}	2.36×10^{-5}	1.14×10^{-2}	-	7.26×10^{-6}	1.39×10^{-4}	5.00×10^{-5}	-	-	-	-
C_4H_4	2.38×10^{-3}	1.64×10^{-4}	2.05×10^{-3}	2.16×10^{-3}	-	-	-	-	-	-	-	-
C_4H_6	9.60×10^{-3}	3.57×10^{-5}	7.57×10^{-3}	8.06×10^{-3}	4.85×10^{-5}	3.27×10^{-5}	2.77×10^{-4}	-	-	-	-	-
C_6H_6	1.64×10^{-4}	5.32×10^{-8}	3.11×10^{-5}	3.76×10^{-5}	1.59×10^{-7}	3.63×10^{-7}	9.24×10^{-6}	-	2.20×10^{-4}	-	-	-
HCN	7.78×10^{-4}	3.25×10^{-11}	5.90×10^{-9}	1.14×10^{-7}	-	7.26×10^{-7}	2.31×10^{-5}	8.50×10^{-6}	6.46×10^{-4}	-	-	-
C_2N_2	1.25×10^{-3}	8.96×10^{-8}	3.83×10^{-6}	8.30×10^{-5}	-	1.09×10^{-7}	2.77×10^{-6}	1.40×10^{-6}	-	-	-	-
CH_3CN	1.59×10^{-3}	2.31×10^{-11}	7.64×10^{-9}	2.42×10^{-7}	-	2.18×10^{-6}	2.77×10^{-5}	6.30×10^{-5}	3.73×10^{-3}	-	-	-
C_2H_3CN	1.44×10^{-2}	5.75×10^{-9}	1.74×10^{-6}	1.54×10^{-4}	-	-	-	2.20×10^{-5}	-	-	-	-
C_2H_5CN	2.49×10^{-2}	9.28×10^{-8}	1.41×10^{-5}	1.25×10^{-3}	-	2.18×10^{-6}	3.70×10^{-5}	8.90×10^{-5}	-	-	-	-
$C_2H_8N_2$	4.87×10^{-4}	2.46×10^{-7}	4.41×10^{-5}	5.44×10^{-5}	-	-	-	-	-	-	-	-
$C_{11}H_{11}N$	4.07×10^{-9}	2.08×10^{-14}	2.09×10^{-10}	2.94×10^{-10}	-	-	-	-	-	-	-	-
H_2O	5.23×10^{-3}	6.17×10^{-20}	5.50×10^{-17}	7.98×10^{-17}	-	1.81×10^{-15}	3.24×10^{-12}	-	-	-	-	-
CO_2	1.06×10^{-3}	3.29×10^{-5}	1.23×10^{-5}	1.32×10^{-5}	2.68×10^{-5}	7.26×10^{-5}	3.24×10^{-5}	1.20×10^{-5}	8.72×10^{-4}	-	-	-

[a] R87: *Raulin* [1987] (graphical reading), D89: *Dubouloz et al.* [1989], C13: *Cordier et al.* [2013b], G13: *Glein and Shock* [2013], T13: *Tan et al.* [2013].

Table C1. Critical Properties of Titanian Materials [*Lide*, 2010][a]

Formula	M (g/mol)	T_c (K)	P_c (MPa)	V_c (cm^3/mol)	Z_{RA}	Z_c
CH_4	16.043	190.564	4.599	98.600	0.289	0.286
C_2H_6	30.069	305.320	4.872	145.500	0.281	0.279
C_3H_8	44.096	369.830	4.248	203.000	0.277	0.280
C_4H_{10}	58.122	425.160	3.787	255.000	0.273	0.273
C_2H_2	26.037	308.300	6.138	112.200	0.271	0.269
C_2H_4	28.053	282.340	5.041	131.000	0.282	0.281
C_3H_4	40.064	402.000	5.630	163.500	0.272	0.275
C_4H_4	52.075	455.600	4.860	218.710	0.282	0.281
C_4H_6	54.091	425.000	4.320	221.000	0.271	0.270
C_6H_6	78.112	562.050	4.895	256.000	0.270	0.268
HCN	27.026	456.700	5.390	139.000	0.197	0.197
C_2N_2	53.034	399.900	6.303	144.520	0.266	0.274
CH_3CN	41.042	545.500	4.850	171.000	0.199	0.183
C_2H_3CN	53.063	536.000	4.559	214.061	0.261	0.219
C_2H_5CN	55.079	561.300	4.260	229.000	0.263	0.209
$C_2H_8N_2$	60.098	522.200	5.400	218.241	0.265	0.271
$C_{11}H_{11}N$	157.212	775.100	3.353	514.500	0.247	0.268
H_2O	18.015	647.140	22.064	56.000	0.233	0.230
CO_2	40.010	304.130	7.375	94.000	0.272	0.274

[a]The Rackett parameters (Z_{RA}) have been gathered from the *CHemical and Engineering Research Information Center* database (http://www.cheric.org/research/kdb/hcprop/cmpsrch.php) and from *Infotherm* (http://www.infotherm.com/servlet/infothermSearch). The compressibility factors (Z_c) have been calculated for comparison with Z_{RA}. The critical properties of cyanogen and our tholins analogs (1-1 dimethyl-hydrazine $C_2H_8N_2$, as suggested in *Cordier et al.* [2013b], based on the experiments of *Quirico et al.* [2008], and quinoline $C_{11}H_{11}N$, as suggested by *Coll et al.* [1995]) have been collected in *Yaws* [1996].

in agreement between our study and others [*Raulin*, 1987; *Dubouloz et al.*, 1989; *Glein and Shock*, 2013] but the solubility of nitriles appears lower in our simulations than in previous ones [*Raulin*, 1987; *Dubouloz et al.*, 1989; *Cordier et al.*, 2013a], for which they lie between our IST and RST estimates.

Appendix C: Molar Volumes of Solvents and Solutes

If the density of a compound at a given temperature (T) is known from experimental data, it is straightforward to derive its molar volume $V_{m,i}(T)$, as follows:

$$V_{m,i}(T) = M_i/\rho_i(T) \qquad (m^3/mol). \tag{C1}$$

This is the case for water ice [*Loerting et al.*, 2011] and minerals [*Lide*, 2010]. However, experimentally determined densities for solids and liquids at the very low temperatures relevant to Titan are rather rare. We describe two complimentary techniques to evaluate the molar volumes of solids and liquids.

C1. Subcooled Liquid Molar Volumes

We first evaluate molar volumes at a given temperature T using the Rackett equation [*Spencer and Danner*, 1972; *Poling et al.*, 2007]. This method is designed to estimate the saturated subcooled liquid molar volumes of pure hydrocarbons and organic solvents ($V^L_{m,i}$).

$$V^L_{m,i} = \frac{R\,T_{c,i}}{P_{c,i}} Z_{c,i}^{\left[1+(1-T_{r,i})^{2/7}\right]} \qquad (m^3/mol). \tag{C2}$$

Table C2. Estimated Subcooled Liquid Molar Volumes (in cm^3/mol) and Associated Mass Densities for Our Best Molar Volume Estimates (in g/cm^3, for Equation (C3) With Z_{RA}) for Titan's Solids and Liquids, Evaluated Using the Rackett Equations and Parameters at 91.5 K

Formula	Equation (C2) (Z_{RA})	Equation (C2) (Z_c)	Equation (C3) (Z_{RA})	Equation (C3) (Z_c)	2σ (Z_{RA})	ρ
CH_4	35.557	34.928	35.212	34.928	0.517	0.456
C_2H_6	46.520	45.968	46.229	45.968	0.456	0.650
C_3H_8	61.390	62.865	62.153	62.865	1.219	0.710
C_4H_{10}	75.882	75.978	75.932	75.978	0.080	0.766
C_2H_2	34.753	34.185	34.453	34.185	0.469	0.756
C_2H_4	42.344	42.147	42.240	42.147	0.162	0.664
C_3H_4	48.267	49.354	48.828	49.354	0.898	0.821
C_4H_4	67.280	66.398	66.824	66.398	0.729	0.779
C_4H_6	65.652	65.175	65.405	65.175	0.394	0.827
C_6H_6	74.256	73.269	73.748	73.269	0.817	1.059
HCN	30.232	30.323	30.279	30.323	0.075	0.893
C_2N_2	41.034	43.436	42.263	43.436	1.987	1.255
CH_3CN	40.219	34.105	36.956	34.105	5.041	1.111
C_2H_3CN	71.655	50.733	60.016	50.733	17.199	0.884
C_2H_5CN	81.023	51.731	64.373	51.731	24.046	0.856
$C_2H_8N_2$	60.828	63.522	62.197	63.522	2.230	0.966
$C_{11}H_{11}N$	123.135	144.275	133.476	144.275	17.564	1.178
H_2O	14.087	13.692	13.884	13.692	0.327	1.298
CO_2	28.789	29.225	29.017	29.225	0.360	1.379

R is the ideal gas constant (= 8.3144621 J/mol/K), T_c and P_c are the critical temperature (in K) and pressure (in Pa or J/m^3), respectively, Z_c is the critical compressibility factor, similar to the Rackett parameter ($Z_{RA} = 0.29056–0.08775\omega$, ω being the accentric factor, see *Poling et al.* [2007] for more details), and T_r the reduced temperature ($T_{r,i} = T/T_{c,i}$). All these parameters are given in Table C1. An alternative form of this equation is given by

$$V^L_{m,i} = V_{c,i} Z_{c,i}^{(1-T_{r,i})^{2/7}} \quad (m^3/mol). \tag{C3}$$

We investigated uncertainties in the molar volumes computed using the Rackett equations (C2) and (C3), with the two different parameters (Z_{RA}, taken from database or computed using the accentric factor, and Z_c, computed from the ideal gas equation at the critical point). The results are reported in Table C2 and Figures C1

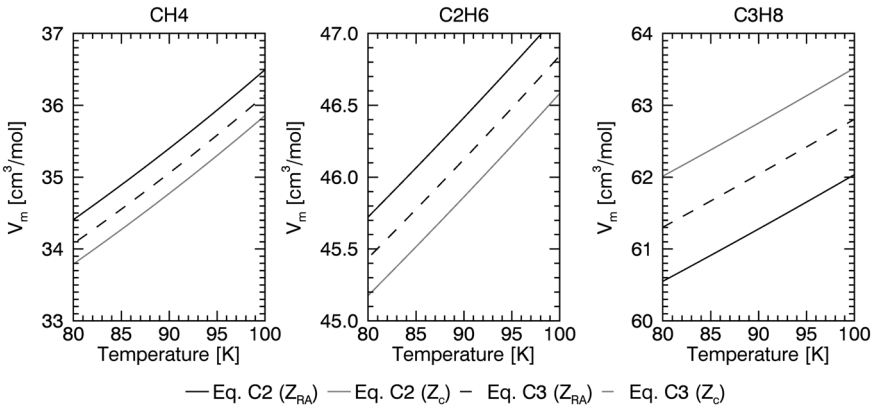

Figure C1. Differences in the calculated molar volumes of Titan's liquids due to the use of different Rackett equations and compressibility factors.

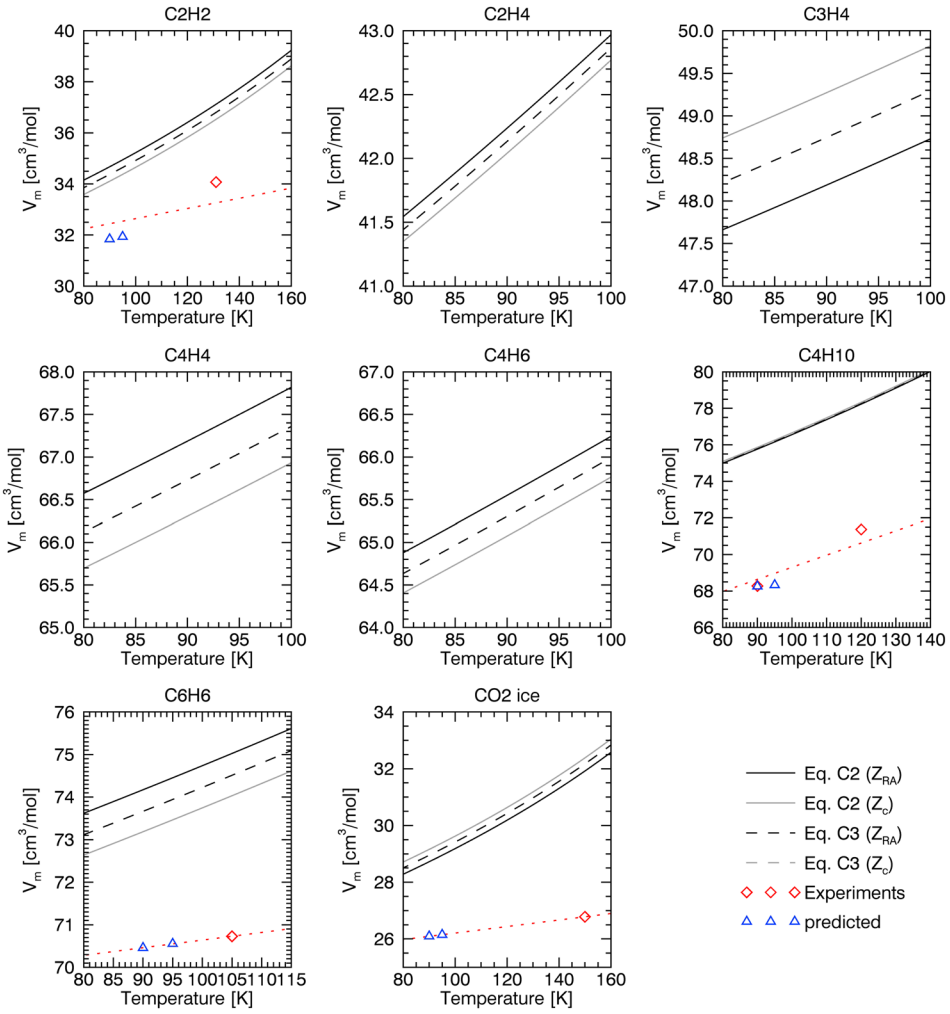

Figure C2. Same as Figure C1 but for "nonpolar" solids (hydrocarbons and carbon dioxide ice). Red and blue diamonds are experimental and predicted values, respectively. Sources: C_4H_{10} [*Refson and Pawley*, 1986], C_2H_2 [*McMullan et al.*, 1992], C_6H_6 [*Craven et al.*, 1993], and CO_2 [*Simon and Peters*, 1980].

(liquids), C2 (nonpolar solids), and C3 (polar solids). Differences in molar volumes are only significant for nitriles, going up to $2\sigma < 24$ cm^3/mol for propionitrile. To reduce possible over or underestimates for nitriles molar volumes and solubilities, we use equation (C3) with Z_{RA}, which is our "intermediate" case and also the most accurate estimates of $V^L_{m,i}$ [*Poling et al.*, 2007].

C2. Titan's Solids Molar Volumes

The solid molar volumes were determined from crystal structures available in the literature [*Dulmage and Lipscomb*, 1951; *Dietrich et al.*, 1975; *Simon and Peters*, 1980; *Refson and Pawley*, 1986; *Antson et al.*, 1987; *Etters and Kuchta*, 1989; *McMullan et al.*, 1992; *Craven et al.*, 1993]. The CH_3CN, HCN, C_4H_{10}, and C_2H_2 have a temperature dependent polymorphism. For each of these compounds, the selected crystal structure corresponds to the one observed at the temperature of Titan's surface (i.e., 90–95 K). Except for CH_3CN, the cell volume was experimentally determined for different temperatures. A second-order polynomial was used to fit the cell volume as a function of the temperature to extrapolate them at Titan's temperatures (90–95 K).

Since the pressure on Titan (around 1.5 bar) is not the same as on Earth (1 bar) where the crystal cell volume were determined, we checked the influence pressure on molar volumes by calculations based on the Density Functional Theory using the Vienna Ab-initio Simulation Package (VASP) 5.3 package. Cell volumes of each compound were optimized using vdW-DF2 [*Lee et al.*, 2010; *Klimeš et al.*, 2011] functional involving a nonlocal kernel for the electronic correlation energy calculation. This functional allows to reproduce dispersion interactions (such as Van der Waals interactions) which are major intermolecular interaction encountered

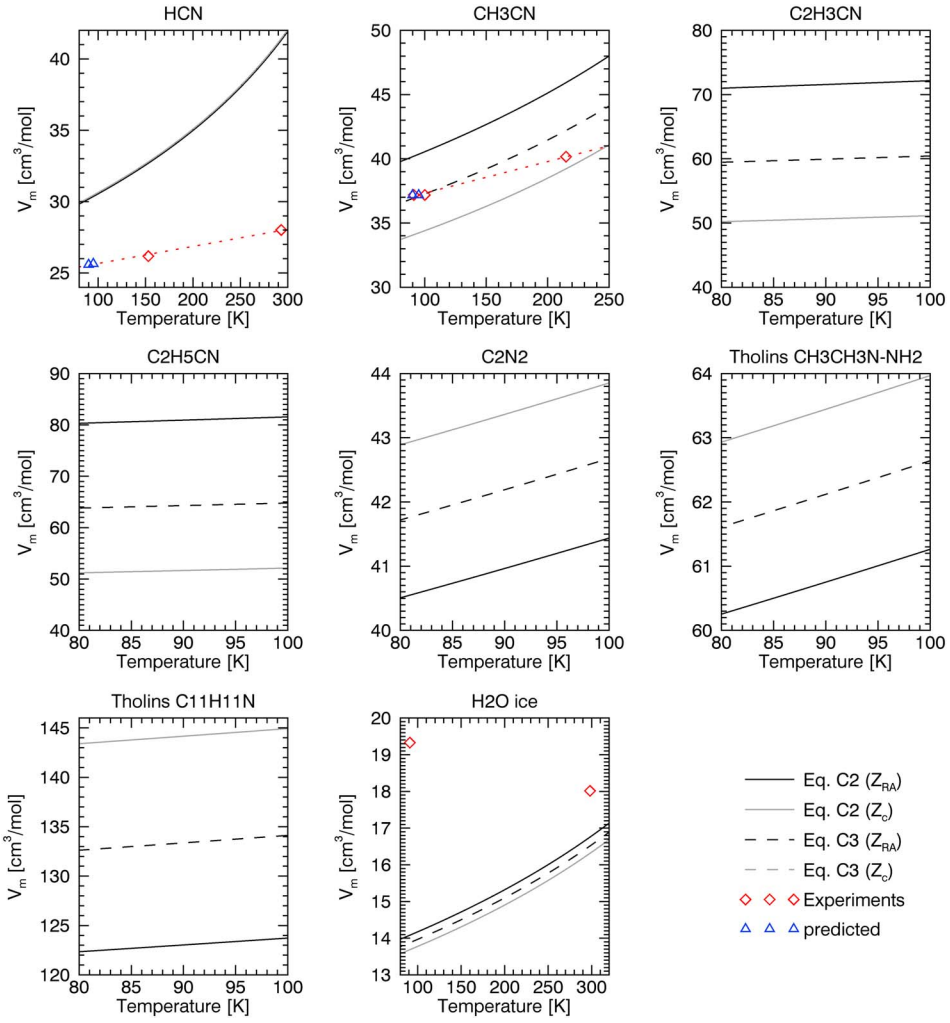

Figure C3. Same as Figure C2 but for polar solids (nitriles and water ice). Sources: HCN [*Dulmage and Lipscomb*, 1951], CH_3CN [*Barrow*, 1981; *Antson et al.*, 1987], and H_2O [*Loerting et al.*, 2011].

in molecular crystals. The E_{ncut} value, defining the basis set size, was fixed to 800 eV in order to suppress Pulay's stress. The *k*-points sampling was done with a 12 × 12 × 12 Monkhorst-Pack grid. The core electrons were described with the projector-augmented plane wave approach. Calculations were performed with and without static pressure (set to 100 bar) to compare cell volumes. The larger variation was observed for C_4H_{10}, with

Table C3. Subcooled Liquid Molar Volumes (in cm^3/mol) and Associated Mass Densities (in g/cm^3) of Titan's Solids Estimated Using the Rackett Equation (C3) With Z_{RA} at 91.5 K Compared to the Solid Molar Volumes (in cm^3/mol) and Associated Mass Densities (in g/cm^3) Computed From an Empirical Linear Fit Between Predictions of the Model and Experimental Data for Some Titanian Materials

Name	Formula	V_m^L (Equation (C3), Z_{RA})	V_m^S (fit)	2σ	ρ^L	ρ^S
n-butane	C_4H_{10}	75.932	68.737	7.195	0.766	0.846
Acetylene	C_2H_2	34.453	32.471	1.982	0.756	0.802
Benzene	C_6H_6	73.748	70.487	3.261	1.059	1.108
Hydrogen cyanide	HCN	30.279	25.562	4.717	0.893	1.057
Acetonitrile	CH_3CN	36.956	37.122	0.166	1.111	1.106
Water ice Ih	H_2O	13.884	19.329	5.446	1.298	0.932
Carbon dioxide ice	CO_2	29.017	26.109	2.909	1.379	1.532

a volume decrease of 0.44% upon pressure. This is reasonably low to conclude that cell volumes measured on Earth (P = 1 bar) should be very similar to the ones on Titan (P = 1.5 bar).

We reported in Figures C2 and C3 the predicted crystalline molar volumes on top of the experimental and Rackett values (individual values also given in Table C3). Overall, we get a quite good agreement between all these estimates. We estimate the solid molar volumes at 91.5 K using a simple empirical linear fit between experimental and predicted points. The Rackett method is used to give an approximate molar volume for the solids for which we do not have experimental data.

Acknowledgments
The Cassini/RADAR SAR imaging data sets are provided through the NASA Planetary Data System Imaging Node portal (http://pds-imaging.jpl.nasa.gov/volumes/radar.html). Terrestrial annual evapotranspiration data taken from the Numerical Terradynamic Simulation Group (NTSG) database (http://ntsg.umt.edu/project/mod16) and precipitation data taken from the WorldClim database (http://www.worldclim.org/current) have been used in this study. The authors want to thank François Raulin and Sébastien Rodriguez for their helpful discussions, Axel Lefèvre and Manuel Giraud for their contribution in the Cassini SAR data processing, and Tim Rawle for the careful proofreading of the manuscript. The authors would like to acknowledge two anonymous reviewers for their work on the preliminary version of the manuscript, as well as the Editor and Associate Editor for useful comments. T.C. is funded by the ESA Postdoctoral Research Fellowship Programme in Space Science.

References

Acocella, V. (2007), Understanding caldera structure and development: An overview of analogue models compared to natural calderas, *Earth Sci. Rev.*, *85*(3–4), 125–160, doi:10.1016/j.earscirev.2007.08.004.

Aharonson, O., A. G. Hayes, J. I. Lunine, R. D. Lorenz, M. D. Allison, and C. Elachi (2009), An asymmetric distribution of lakes on Titan as a possible consequence of orbital forcing, *Nat. Geosci.*, *2*, 851–854, doi:10.1038/ngeo698.

Antson, O., K. Tilli, and N. Andersen (1987), Neutron powder diffraction study of deuterated b-acetonitrile, *Acta Crystallogr., Sect. B: Struct. Sci.*, *43*, 296–301, doi:10.1107/S0108768187097866.

Atreya, S. K. (2007), Titan's organic factory, *Science*, *316*(5826), 843–845, doi:10.1126/science.1141869.

Barnes, J. W., R. H. Brown, L. Soderblom, B. J. Buratti, C. Sotin, S. Rodriguez, S. Le Mouélic, K. H. Baines, R. Clark, and P. Nicholson (2007), Global-scale surface variations on Titan seen from Cassini/VIMS, *Icarus*, *186*(1), 242–258, doi:10.1016/j.icarus.2006.08.021.

Barnes, J. W., et al. (2009), Shoreline features of Titan's Ontario Lacus from Cassini/VIMS observations, *Icarus*, *201*(1), 217–225, doi:10.1016/j.icarus.2008.12.028.

Barnes, J. W., et al. (2011), Organic sedimentary deposits in Titan's dry lakebeds: Probable evaporite, *Icarus*, *216*(1), 136–140, doi:10.1016/j.icarus.2011.08.022.

Barrow, M. (1981), A-acetonitrile at 215 K, *Acta Crystallogr., Sect. B: Struct. Sci.*, *37*, 2239–2242, doi:10.1107/S0567740881008510.

Black, B. A., J. T. Perron, D. M. Burr, and S. A. Drummond (2012), Estimating erosional exhumation on Titan from drainage network morphology, *J. Geophys. Res.*, *117*, E08006, doi:10.1029/2012JE004085.

Bourgeois, O., T. Lopez, S. Le Mouélic, C. Fleurant, G. Tobie, L. Le Corre, L. Le Deit, C. Sotin, and Y. Bodeur (2008), A surface dissolution/precipitation model for the development of lakes on Titan, based on an arid terrestrial analogue: The Pans and Calcretes of Etosha, *Lunar Planet. Sci. Conf. 39th*, p. 1733.

Bowen, M. W., and W. C. Johnson (2012), Late Quaternary environmental reconstructions of playa-lunette system evolution on the central High Plains of Kansas, United States, *Geol. Soc. Am. Bull.*, *124*(1), 146–161, doi:10.1130/B30382.1.

Brew, T. C. L. (1977), A study on the solubility of heavy hydrocarbons in liquid methane and methane containing mixtures, Master's thesis, Univ. of Ottawa, Canada.

Brezonik, P., and W. Arnold (2011), *Water Chemistry: An Introduction to the Chemistry of Natural and Engineered Aquatic Systems*, 809 pp., Oxford Univ. Press, New York.

Brown, R. H., L. A. Soderblom, J. M. Soderblom, R. N. Clark, R. Jaumann, J. W. Barnes, C. Sotin, B. Buratti, K. H. Baines, and P. D. Nicholson (2008), The identification of liquid ethane in Titan's Ontario Lacus, *Nature*, *454*, 607–610, doi:10.1038/nature07100.

Buch, M. W. (1997), Etosha Pan—The third largest lake in the world?, *Madoqua*, *20*(1), 49–64.

Buch, M. W., and D. Rose (1996), Mineralogy and geochemistry of the sediments of the Etosha Pan Region in northern Namibia: A reconstruction of the depositional environment, *J. Afr. Earth. Sci.*, *22*(3), 355–378, doi:10.1016/0899-5362(96)00020-6.

Buch, M. W., and C. Trippner (1997), Overview of the geological and geomorphological evolution of the Etosha region, Northern Namibia, *Madoqua*, *20*(1), 65–74.

Cabane, M., E. Chassefière, and G. Israel (1992), Formation and growth of photochemical aerosols in Titan's atmosphere, *Icarus*, *96*(2), 176–189, doi:10.1016/0019-1035(92)90071-E.

Cheung, H., and E. H. Zander (1968), Solubility of carbon dioxide and hydrogen sulfide in liquid hydrocarbons at cryogenic temperatures, *Chem. Eng. Prog.*, *64*(88), 33–34.

Chevrier, V., S. Singh, D. Nna-Mvondo, D. Mège, M. Leitner, and A. Wagner (2014), Solubility and detection of simple and complex organics in Titan's liquid hydrocarbons, in *Titan Through Time—3rd Workshop*, pp. 14–15.

Chirico, R. D., R. D. J. III, and W. V. Steele (2007), Thermodynamic properties of methylquinolines: Experimental results for 2,6-dimethylquinoline and mutual validation between experiments and computational methods for methylquinolines, *J. Chem. Thermodyn.*, *39*(5), 698–711, doi:10.1016/j.jct.2006.10.012.

Choukroun, M., and C. Sotin (2012), Is Titan's shape caused by its meteorology and carbon cycle?, *Geophys. Res. Lett.*, *39*, L04201, doi:10.1029/2011GL050747.

Clark, A. M., and F. Din (1953), Equilibria between solid, liquid and gaseous phases at low temperatures. The system carbon dioxide + ethane + ethylene, *Discuss. Faraday Soc.*, *15*, 202–207.

Clark, R. N., et al. (2010), Detection and mapping of hydrocarbon deposits on Titan, *J. Geophys. Res.*, *115*, E10005, doi:10.1029/2009WR008896.

Coll, P., D. Cosia, M.-C. Gazeau, E. de Vanssay, J.-C. Guillemin, and F. Raulin (1995), Organic chemistry in Titan's atmosphere: New data from laboratory simulations at low temperature, *Adv. Space Res.*, *16*(2), 93–103, doi:10.1016/0273117(95)00197-M.

Cordier, D., O. Mousis, J. I. Lunine, P. Lavvas, and V. Vuitton (2009), An estimate of the chemical composition of Titan's lakes, *Astrophys. J.*, *707*, L128–L131, doi:10.1088/0004-637X/707/2/L128.

Cordier, D., O. Mousis, J. I. Lunine, P. Lavvas, and V. Vuitton (2013a), Erratum: An estimate of the chemical composition of Titan's lakes, *Astrophys. J. Lett.*, *768*, L23, doi:10.1088/2041-8205/768/1/L23.

Cordier, D., J. Barnes, and A. Ferreira (2013b), On the chemical composition of Titan's dry lakebed evaporites, *Icarus*, *226*(2), 1431–1437, doi:10.1016/j.icarus.2013.07.026.

Cornet, T., et al. (2012), Geomorphological significance of Ontario Lacus on Titan: Integrated interpretation of Cassini VIMS, ISS and RADAR data and comparison with the Etosha Pan (Namibia), *Icarus*, *218*(2), 788–806, doi:10.1016/j.icarus.2012.01.013.

Cottini, V., et al. (2012), Water vapor in Titan's stratosphere from Cassini CIRS far-infrared spectra, *Icarus*, *220*(2), 855–862, doi:10.1016/j.icarus.2012.06.014.

Coustenis, A., et al. (2010), Titan trace gaseous composition from CIRS at the end of the Cassini-Huygens prime mission, *Icarus*, *207*(1), 461–476, doi:10.1016/j.icarus.2009.11.027.

Craven, C., P. Hatton, C. Howard, and G. Pawley (1993), The structure and dynamics of solid benzene. I. A neutron powder diffraction study of deuterated benzene from 4 K to the melting point, *J. Chem. Phys.*, *98*, 8236–8243.
Cui, J., et al. (2009), Analysis of Titan's neutral upper atmosphere from Cassini Ion Neutral Mass Spectrometer measurements, *Icarus*, *200*(2), 581–615, doi:10.1016/j.icarus.2008.12.005.
Davis, J. A., N. Rodewald, and F. Kurata (1962), Solid-liquid-vapor phase behavior of the methane-carbon dioxide system, *AIChE J.*, *8*(4), 537–539, doi:10.1002/aic.690080423.
Dietrich, O., G. Mackenzie, and G. Pawley (1975), The structural phase transition in solid DCN, *J. Phys. C: Solid State Phys.*, *8*, L98, doi:10.1088/0022-3719/8/7/002.
Dubouloz, N., F. Raulin, E. Lellouch, and D. Gautier (1989), Titan's hypothesized ocean properties: The influence of surface temperature and atmospheric composition uncertainties, *Icarus*, *82*(1), 81–96, doi:10.1016/0019-1035(89)90025-0.
Dulmage, W., and W. Lipscomb (1951), The crystal structures of hydrogen cyanide, HCN, *Acta Crystallogr.*, *4*, 330–334, doi:10.1107/S0365110X51001070.
Etters, R., and B. Kuchta (1989), Static and dynamic properties of solid CO2 at various temperatures and pressures, *J. Chem. Phys.*, *90*, 4537–4551, doi:10.1063/1.456640.
Fleurant, C., G. Tucker, and H. Viles (2008), A cockpit karst evolution model, in *Landscape Evolution: Denudation, Climate and Tectonics Over Different Time and Space Scales*, vol. 296, edited by Gallagher, K., S. J. Jones, and J. Wainwright, pp. 47–62, Geol. Soc. of London, doi: 10.1144/SP296.4.
Ford, D., and P. Williams (2007), *Karst Hydrogeology and Geomorphology*, 562 pp., John Wiley, Chichester, West Sussex, England.
French, H. M. (2007), *The Periglacial Environment*, 3rd ed., 458 pp., John Wiley, Chichester, West Sussex, England.
Frumkin, A. (1994), Hydrology and denudation rates of halite karst, *J. Hydrol.*, *162*, 171–189, doi:10.1016/0022-1694(94)90010-8.
Frumkin, A. (1996), Uplift rate relative to base-levels of a salt diapir (Dead Sea Basin, Israel) as indicated by cave levels, *Geol. Soc. Spec. Publ.*, *100*, 41–47, doi:10.1144/GSL.SP.1996.100.01.04.
Garasic, M. (2001), New speleohydrogeological research of Crveno jezero (Red Lake) near Imotski in Dinaric Karst Area (Croatia, Europe)—International speleodiving expedition "Crveno jezero 98', *13th International Congress of Speleology, 4th Speleological Congress of Latin América and Caribbean, 26th Brazilian Congress of Speleology*, pp. 555–559.
Garasic, M. (2012), Crveno Jezero—The biggest sinkhole in Dinaric Karst (Croatia), in *EGU General Assembly Conference Abstracts*, edited by A. Abbasi, and N. Giesen, pp. 7132–7134.
Glein, C. R., and E. L. Shock (2013), A geochemical model of non-ideal solutions in the methane-ethane-propane-nitrogen-acetylene system on Titan, *Geochim. Cosmochim. Acta*, *115*, 217–240, doi:10.1016/j.gca.2013.03.030.
Goudie, A. S., and G. L. Wells (1995), The nature, distribution and formation of pans in arid zones, *Earth Sci. Rev.*, *38*, 1–69, doi:10.1016/0012-8252(94)00066-6.
Graves, S. D. B., C. P. McKay, C. A. Griffith, F. Ferri, and M. Fulchigoni (2008), Rain and hail can reach the surface of Titan, *Planet. Space Sci.*, *56*, 346–357, doi:10.1016/j.pss.2007.11.001.
Harrisson, K. P. (2012), Thermokarst processes in Titan's lakes: Comparison with terrestrial data, *Lunar Planet. Sci. Conf. 43rd*, pp. 2271–2272.
Hayes, A., et al. (2008), Hydrocarbon lakes on Titan: Distribution and interaction with an isotropic porous regolith, *Geophys. Res. Lett.*, *35*, L09204, doi:10.1029/2008GL033409.
Heintz, A., and E. Bich (2009), Thermodynamics in an icy world: The atmosphere and internal structure of Saturn's moon Titan, *Pure Appl. Chem.*, *81*(10), 1903–1920, doi:10.1351/PAC-CON-08-10-04.
Hipondoka, M. H. T. (2005), The development and evolution of Etosha Pan, Namibia, PhD thesis, 154 pp., Univ. of Wurzburg, Germany.
Jennings, D. E., et al. (2009), Titan's surface brightness temperatures, *Astrophys. J. Lett.*, *691*(2), L103–L105, doi:10.1088/0004-637X/691/2/L103.
Kargel, J. S., R. Furfaro, C. C. Hays, R. M. C. Lopes, J. I. Lunine, K. L. Mitchell, S. D. Wall, and Cassini RADAR Team (2007), Titan's GOO-sphere: Glacial, permafrost, evaporite, and other familiar processes involving exotic materials, *Lunar Planet. Sci. Conf. 38th*, pp. 1992–1993.
Kirk, R. L., and E. Howington-Kraus (2008), Radargrammetry on three planets, *Int. Arch. Photogramm. Remote Sens.*, *37*(B4), 973–980.
Kirk, R. L., E. Howington-Kraus, K. L. Mitchell, S. Hensley, B. W. Stiles, and Cassini RADAR Team (2007), First stereoscopic radar images of Titan, *Lunar Planet. Sci. Conf. 38th*, pp. 1427–1428.
Kirk, R. L., et al. (2012), Topographic mapping of Titan: Latest results, *Lunar Planet. Sci. Conf. 43rd*, pp. 2759–2760.
Klimeš, J., D. R. Bowler, and A. Michaelides (2011), Van Der Waals density functionals applied to solids, *Phys. Rev. B*, *83*, 195131, doi:10.1103/PhysRevB.83.195131.
Krasnopolsky, V. A. (2009), A photochemical model of Titan's atmosphere and ionosphere, *Icarus*, *201*(1), 226–256, doi:10.1016/j.icarus.2008.12.038.
Kuebler, G. P., and G. McKinley (1975), Solubility of solid n-butane and n-pentane in liquid methane, in *Advances in Cryogenic Engineering*, vol. 21, pp. 509–515, Springer, doi:10.1007/978-1-4757-0208-8_60.
Kuebler, G. P., and G. McKinley (1995), Solubility of solid benzene, toluene, n-hexane, n-heptane, in liquid methane, in *Advances in Cryogenic Engineering*, vol. 19, pp. 320–326, Springer, doi:10.1007/978-1-4613-9847-9_39.
Langmuir, D. (1997), *Aqueous Environmental Geochemistry*, 618 pp., Prentice Hall, Upper Saddle River, N. J.
Lara, L. M., E. Lellouch, J. J. López-Moreno, and R. Rodrigo (1996), Vertical distribution of Titan's atmospheric neutral constituents, *J. Geophys. Res.*, *101*(E10), 23,161–23,283, doi:10.1029/96JE02036.
Lavvas, P. P., A. Coustenis, and I. M. Vardavas (2008a), Coupling photochemistry with haze formation in Titan's atmosphere, Part I: Model description, *Planet. Space Sci.*, *56*(1), 27–66, doi:10.1016/j.pss.2007.05.026.
Lavvas, P. P., A. Coustenis, and I. M. Vardavas (2008b), Coupling photochemistry with haze formation in Titan's atmosphere, Part II: Results and validation with Cassini/Huygens data, *Planet. Space Sci.*, *56*(1), 67–99, doi:10.1016/j.pss.2007.05.027.
Lee, K., E. D. Murray, L. Kong, B. I. Lundqvist, and D. C. Langreth (2010), Higher-accuracy Van der Waals density functional, *Phys. Rev. B*, *82*, 081101, doi:10.1103/PhysRevB.82.081101.
Leitner, M., S. Singh, and V. F. Chevrier (2014), Solubility and detectability of acetonitrile in Titan lakes, *Lunar Planet. Sci. Conf. 45th*, p. 2658.
Lide, D. (2010), *CRC Handbook of CHemistry and Physics*, 90th ed. (CD-ROM version 2010), CRC Press/Taylor and Francis, Boca Raton, Fla.
Loerting, T., M. Bauer, I. Kohl, K. Watschinger, K. Winkel, and E. Mayer (2011), Cryoflotation: Densities of amorphous and crystalline ices, *J. Phys. Chem. B*, *115*, 14,167–14,175, doi:10.1021/jp204752w.
Lopes, R. M. C., et al. (2007), The lakes and seas of Titan, *Eos Trans. AGU*, *88*(51), 569–576, doi:10.1029/2007EO510001.
Lora, J. M., P. J. Goodman, J. L. Russell, and J. I. Lunine (2011), Insolation in Titan's troposphere, *Icarus*, *216*(1), 116–119, doi:10.1016/j.icarus.2011.08.017.
Lorenz, R. D., and J. I. Lunine (2002), Titan's snowline, *Icarus*, *158*(2), 557–559, doi:10.1006/icar.2002.6880.
Lorenz, R. D., et al. (2008), Titan's inventory of organic surface materials, *Geophys. Res. Lett.*, *35*, L02206, doi:10.1029/2007GL03118.
Lorenz, R. D., et al. (2013), A global topographic map of Titan, *Icarus*, *225*(1), 367–377, doi:10.1016/j.icarus.2013.04.002.

Lorenz, R. D., et al. (2014), A Radar map of Titan seas: Tidal dissipation and ocean mixing through the throat of Kraken, *Icarus*, *237*, 9–15, doi:10.1016/j.icarus.2014.04.005.
Lorenz, V. (1986), On the growth of maars and diatremes and its relevance to the formation of tuff rings, *Bull. Volcanol.*, *48*, 265–274, doi:10.1007/BF01081755.
Luks, K. D., J. D. Hottovy, and J. P. Kohn (1981), Three-phase solid-liquid-vapor equilibriums in the binary hydrocarbon systems methane-n-hexane and methane-benzene, *J. Chem. Eng. Data*, *26*(4), 402–403, doi:10.1021/je00026a016.
Lunine, J. I., D. J. Stevenson, and Y. L. Yung (1983), Ethane ocean on Titan, *Science*, *222*(4629), 1229–1230, doi:10.1126/science.222.4629.1229.
Lunine, J. I., et al. (2008), Titan's diverse landscapes as evidenced by Cassini Radar's third and fourth looks at Titan, *Icarus*, *195*(1), 415–433, doi:10.1016/j.icarus.2007.12.022.
Luspay-Kuti, A., V. F. Chevrier, F. C. Wasiak, L. A. Roe, W. D. D. P. Welivitiya, T. Cornet, S. Singh, and E. G. Rivera-Valentin (2012), Experimental simulations of CH_4 evaporation on Titan, *Geophys. Res. Lett.*, *39*, L23808, doi:10.1029/2012GL054003.
Luspay-Kuti, A., V. F. Chevrier, D. Cordier, E. G. Rivera-Valentin, S. Singh, A. Wagner, and F. Wasiak (2014), Experimental constraints on the composition and dynamics of Titan's polar lakes, *Earth Planet. Sci. Lett.*, *410*, 75–83, doi:10.1016/j.epsl.2014.11.023.
Lyew-Ayee, P. (2010), *The Cockpit Country of Jamaïca: An Island Within an Island*, pp. 69–77, Springer, Dordrecht, Heidelberg, London, and New York, doi:10.1007/978-90-481-3055-9_8.
MacKenzie, S. M., et al. (2014), Evidence of Titan's climate history from evaporite distribution, *Icarus*, *243*, 191–207, doi:10.1016/j.icarus.2014.08.022.
Magee, B. A., J. H. Waite, K. E. Mandt, J. Westlake, J. Bell, and D. A. Gell (2009), INMS-derived composition of Titan's upper atmosphere: Analysis methods and model comparison, *Planet. Space Sci.*, *57*(14–15), 1895–1916, doi:10.1016/j.pss.2009.06.016.
Malaska, M., J. Radebaugh, R. Lorenz, K. Mitchell, T. Farr, and E. Stofan (2010), Identification of karst-like terrain on Titan from valley analysis, *Lunar Planet. Sci. Conf. 41st*, pp. 1544–1545.
Malaska, M., J. Radebaugh, K. Mitchell, R. Lopes, S. Wall, and R. Lorenz (2011), Surface dissolution model for Titan karst, in *First International Planetary Cave Research Workshop*, pp. 8018–8019.
Malaska, M. J., and R. Hodyss (2014), Dissolution of benzene, naphthalene, and biphenyl in a simulated Titan lake, *Icarus*, *242*, 74–81, doi:10.1016/j.icarus.2014.07.022.
Mastrogiuseppe, M., et al. (2014), The bathymetry of a Titan sea, *Geophys. Res. Lett.*, *41*, 1432–1437, doi:10.1002/2013GL058618.
McMullan, R., A. Kvick, and P. Popelier (1992), Structures of cubic and orthorhombic phases of acetylene by single-crystal neutron diffraction, *Acta Crystallogr., Sect. B: Struct. Sci*, *48*, 726–731, doi:10.1107/S0108768192004774.
Mihevc, A., M. Prelovsek, and N. Zupan Hajna (Eds.) (2010), *Introduction to the Dinaric Karst*, 72 pp., Karst Res. Inst., ZRC SAZU, Postojna, Slovenia.
Miller, R. M., M. Pickford, and B. Senut (2010), The geology, palaeontology and evolution of the Etosha Pan, Namibia: Implications for terminal Kalahari deposition, *S. Afr. J. Geol.*, *113*(3), 307–334, doi:10.2113/gssajg.113.307.
Mitchell, J. L. (2008), The drying of Titan's dunes: Titan's methane hydrology and its impact on atmospheric circulation, *J. Geophys. Res.*, *113*, E08015, doi:10.1029/2007JE003017.
Mitchell, J. L., R. T. Pierrehumbert, D. M. Frierson, and R. Caballero (2009), The impact of methane thermodynamics on seasonal convection and circulation in a model Titan atmosphere, *Icarus*, *203*(1), 250–264, doi:10.1016/j.icarus.2009.03.043.
Mitchell, J. L., M. Ádámkovics, R. Caballero, and E. P. Turtle (2011), Locally enhanced precipitation organized by planetary-scale waves on Titan, *Nat. Geosci.*, *4*, 589–592, doi:10.1038/ngeo1219.
Mitchell, K. L., and M. Malaska (2011), Karst on Titan, in *First International Planetary Cave Research Workshop*, pp. 8021–8022.
Mitchell, K. L., J. S. Kargel, C. A. Wood, J. Radebaugh, R. M. C. Lopes, J. I. Lunine, E. R. Stofan, R. L. Kirk, and Cassini RADAR Team (2007), Titan's crater lakes: Caldera vs. karst?, *Lunar Planet. Sci. Conf. 38th*, pp. 2061–2064.
Moore, J. M., and A. D. Howard (2010), Are the basins of Titan's Hotei Regio and Tui Regio sites of former low latitude seas?, *Geophys. Res. Lett.*, *37*, L22205, doi:10.1029/2010GL045234.
Moore, J. M., and R. T. Pappalardo (2011), Titan: An exogenic world?, *Icarus*, *212*(2), 790–806, doi:10.1016/j.icarus.2011.01.019.
Moriconi, M. L., J. I. Lunine, A. Adriani, E. D'Aversa, A. Negrao, G. Filacchione, and A. Coradini (2010), Characterization of Titan's Ontario Lacus region from Cassini/VIMS observations, *Icarus*, *210*(2), 823–831, doi:10.1016/j.icarus.2010.07.023.
Neish, C. D., and R. D. Lorenz (2012), Titan's global crater population: A new assessment, *Planet. Space Sci.*, *60*(1), 26–33, doi:10.1016/j.pss.2011.02.016.
Neumann, A., and R. Mann (1969), Die Löslichkeit von festem Acetylen in flüssigen Methan/Äthylen-Mischungen, *Chem. Ing. Tech.*, *41*(12), 708–711, doi:10.1002/cite.330411204.
Poling, B. E., J. M. Prausnitz, and J. P. O'Connell (2007), *The Properties of Gases and Liquids*, 5th ed., McGraw-Hill Prof., Englewood Cliffs, N. J.
Preston, G. T., and J. M. Prausnitz (1970), Thermodynamics of solid solubility in cryogenic solvents, *Ind. Eng. Chem. Process Des. Dev.*, *9*(2), 264–271, doi:10.1021/i260034a017.
Preston, G. T., E. W. Funk, and J. M. Prausnitz (1971), Solubilities of hydrocarbons and carbon dioxide in liquid methane and in liquid argon, *J. Phys. Chem.*, *75*(15), 2345–2352.
Quirico, E., et al. (2008), New experimental constraints on the composition and structure of tholins, *Icarus*, *198*(1), 218–231, doi:10.1016/j.icarus.2008.07.012.
Rannou, P., C. P. McKay, and R. D. Lorenz (2003), A model of Titan's haze of fractal aerosols constrained by multiple observations, *Planet. Space Sci.*, *51*(14–15), 963–976, doi:10.1016/j.pss.2003.05.008.
Rannou, P., F. Montmessin, F. Hourdin, and S. Lebonnois (2006), The latitudinal distribution of clouds on Titan, *Science*, *311*, 201–205, doi:10.1126/science.1118424.
Raulin, F. (1987), Organic chemistry in the oceans of Titan, *Adv. Space Res.*, *7*(5), 571–581, doi:10.1016/0273-1177(87)90358-9.
Refson, K., and G. Pawley (1986), The structure and orientational disorder in solid n-butane by neutron powder diffraction, *Acta Crystallogr., Sect. B: Struct. Sci.*, *42*, 402–410, doi:10.1107/S010876818609804X.
Rodriguez, S., et al. (2009), Global circulation as the main source of cloud activity on Titan, *Nature*, *459*, 678–682, doi:10.1038/nature08014.
Rodriguez, S., et al. (2011), Titan's cloud seasonal activity from winter to spring with Cassini/VIMS, *Icarus*, *216*(1), 89–110, doi:10.1016/j.icarus.2011.07.031.
Rodriguez, S., et al. (2014), Global mapping and characterization of Titan's dune fields with Cassini: Correlation between {RADAR} and {VIMS} observations, *Icarus*, *230*, 168–179, doi:10.1016/j.icarus.2013.11.017.
Roe, H. G., I. de Pater, B. A. Macintosh, S. G. Gibbard, C. E. Max, and C. P. McKay (2002), Titan's atmosphere in late southern spring observed with adaptive optics on the W. M. Keck II 10-meter telescope, *Icarus*, *157*(1), 254–258, doi:10.1006/icar.2002.6831.
Schaller, E. L., M. E. Brown, H. G. Roe, and A. H. Bouchez (2006), A large cloud outburst at Titan's south pole, *Icarus*, *182*(1), 224–229, doi:10.1016/j.icarus.2005.12.021.

Schaller, E. L., H. G. Roe, T. Schneider, and M. E. Brown (2009), Storms in the tropics of Titan, *Nature*, *460*(7257), 873–875, doi:10.1038/nature08193.

Schneider, T., S. D. B. Graves, E. L. Schaller, and M. E. Brown (2012), Polar methane accumulation and rainstorms on Titan from simulations of the methane cycle, *Nature*, *481*, 58–61, doi:10.1038/nature10666.

Sharma, P., and S. Byrne (2010), Constraints on Titan's topography through fractal analysis of shorelines, *Icarus*, *209*, 723–737, doi:10.1016/j.icarus.2010.04.023.

Sharma, P., and S. Byrne (2011), Comparison of Titan's north polar lakes with terrestrial analogs, *Geophys. Res. Lett.*, *38*, L24203, doi:10.1029/2011GL049577.

Shaw, P. A., and D. S. G. Thomas (2000), Pans, playas and salt lakes, in *Arid Zone Geomorphology: Process, Form and Change in Drylands*, edited by D. S. G. Thomas, 2nd ed., chap. 15, pp. 293–317, John Wiley, England.

Simon, A., and K. Peters (1980), Single-crystal refinement of the structure of carbon dioxide, *Acta Crystallogr., Sect. B: Struct. Sci*, *36*, 2750–2751, doi:10.1107/S0567740880009879.

Singh, S., V. F. Chevrier, A. Wagner, M. Leitner, M. Gainor, L. Roe, T. Cornet, and J.-P. Combe (2014), Solubility of acetylene in liquid hydrocarbons under Titan surface conditions, *Lunar Planet. Sci. Conf. 45th*, p. 2850.

Sket, B. (2012), Diversity patterns in the Dinaric Karst, in *Encyclopedia of Caves*, edited by W. B. White, and D. C. Cluver, pp. 228–238, Elsevier Inc., Amsterdam.

Sotin, C., et al. (2012), Observations of Titan's northern lakes at 5 microns: Implications for the organic cycle and geology, *Icarus*, *221*(2), 768–786, doi:10.1016/j.icarus.2012.08.017.

Spencer, C. F., and R. P. Danner (1972), Improved equation for prediction of saturated liquid density, *J. Chem. Eng. Data*, *17*, 236–241, doi:10.1021/je60053a012.

Stephan, K. et al. (2009), Titan from Cassini-Huygens, in *Mapping Products of Titan's Surface*, edited by R. H. Brown, J.-P. Lebreton, and J. H. Waite, pp. 489–510, Springer, Netherlands, doi:10.1007/978-1-4020-9215-2.

Stiles, B. W., et al. (2009), Determining Titan surface topography from Cassini SAR data, *Icarus*, *202*(2), 584–598, doi:10.1016/j.icarus.2009.03.032.

Stofan, E. R., et al. (2007), The lakes of Titan, *Nature*, *445*, 61–64, doi:10.1038/nature05438.

Szczepaniec-Cieciak, E., B. Dabrowska, J. M. Lagan, and Z. Wojtaszek (1978), Estimation of the solubility of solidified substances in liquid methane by the Preston-Prausnitz method, *Cryogenics*, *18*(10), 591–600, doi:10.1016/0011-2275(78)90186-8.

Tan, S. P., J. S. Kargel, and G. M. Marion (2013), Titan's atmosphere and surface liquid: New calculation using statistical associating fluid theory, *Icarus*, *222*(1), 53–72, doi:10.1016/j.icarus.2012.10.032.

Tewelde, Y., J. T. Perron, P. Ford, S. Miller, and B. Black (2013), Estimates of fluvial erosion on titan from sinuosity of lake shorelines, *J. Geophys. Res. Planets*, *118*, 2198–2212, doi:10.1002/jgre.20153.

Tobie, G., J. I. Lunine, and C. Sotin (2006), Episodic outgassing as the origin of atmospheric methane on Titan, *Nature*, *440*(7080), 61–64, doi:10.1038/nature04497.

Tokano, T. (2009), Impact of seas/lakes on polar meteorology of Titan: Simulation by a coupled GCM-Sea model, *Icarus*, *204*(2), 619–636, doi:10.1016/j.icarus.2009.07.032.

Toublanc, D., J. P. Parisot, J. Brillet, D. Gautier, F. Raulin, and C. P. McKay (1995), Photochemical modeling of Titan's atmosphere, *Icarus*, *113*(1), 2–26, doi:10.1006/icar.1995.1002.

Truesdell, A., and B. Jones (1974), WATEQ, a computer program for calculating chemical equilibria of natural waters, *J. Res. U.S. Geol. Surv.*, *2*, 233–248.

Tucker, G. E., S. T. Lancaster, N. M. Gasparini, and R. L. Bras (2001), The Channel-Hillslope Integrated Landscape Development (CHILD) model, in *Landscape Erosion and Evolution Modeling*, edited by R. S. Harmon, and W. W. Doe III, pp. 349–388, Springer.

Turtle, E. P., et al. (2011a), Rapid and extensive surface changes near Titan's equator: Evidence of April showers, *Science*, *331*, 1414–1417, doi:10.1126/science.1201063.

Turtle, E. P., A. D. Del Genio, J. M. Barbara, J. E. Perry, E. L. Schaller, A. S. McEwen, R. A. West, and T. L. Ray (2011b), Seasonal changes in Titan's meteorology, *Geophys. Res. Lett.*, *38*, L03203, doi:10.1029/2010GL046266.

Vinatier, S., et al. (2010), Analysis of Cassini/CIRS limb spectra of Titan acquired during the nominal mission: I. Hydrocarbons, nitriles and CO2 vertical mixing ratio profiles, *Icarus*, *205*(2), 559–570, doi:10.1016/j.icarus.2009.08.013.

Vixie, G., J. W. Barnes, B. Jackson, and P. Wilson (2012), Temperate lakes discovered on Titan, *Lunar Planet. Sci. Conf. 43rd*, p. 2766.

Vlahovic, I., J. Tisljar, I. Velic, and D. Maticec (2002), The Karst Dinarides are composed of relics of a single Mesozoic platform: Facts and consequences, *Geol. Croat.*, *55*(2), 171–183.

von Szalghary, W.-D. (1972), Löslichkeit von festem benzol in flüssigen Kohlenwasserstoffen, *Kältetechnik-Klimatisierung*, *24*, 145–149.

Waltham, T. (2008), Fengcong, fenglin, cone karst and tower karst, *Cave Karst Sci.*, *35*, 77–88.

Wang, P., and Q. Li (2009), Monsoons: Pre-quaternary, in *Encyclopedia of Paleoclimatology and Ancient Environments*, edited by V. Gornitz, pp. 583–589, Springer, Netherlands.

Wasiak, F. C., D. Androes, D. G. Blackburn, J. A. Tullis, J. Dixon, and V. F. Chevrier (2013), A geological characterization of Ligeia Mare in the northern polar region of Titan, *Planet. Space Sci.*, *84*, 141–147, doi:10.1016/j.pss.2013.05.007.

White, W. B. (1984), Rate processes: Chemical kinetics and karst landform development, in *Groundwater as a Geomorphic Agent*, pp. 227–248, Allen and Unwin, Inc, Boston, Mass.

White, W. B. (2012), Hydrogeology of karst aquifers, in *Encyclopedia of Caves*, 2nd edn., pp. 383–391, Elsevier, Amsterdam.

White, W. M. (2013), *Geochemistry*, 672 pp., John Wiley, New York.

Wilson, E. H., and S. K. Atreya (2004), Current state of modeling the photochemistry of Titan's mutually dependent atmosphere and ionosphere, *J. Geophys. Res.*, *109*, E06002, doi:10.1029/2003JE002181.

Wood, C. A., K. L. Mitchell, R. M. C. Lopes, J. Radebaugh, E. Stofan, J. Lunine, and Cassini RADAR Team (2007), Volcanic calderas in the north polar region of Titan, *Lunar Planet. Sci. Conf. 38th*, pp. 1454–1455.

Xuewen, Z., and C. Weihai (2006), Tiankengs in the karst of China, *Speleogenesis Evol. Karst Aquifers*, *4*(1), 1–18.

Yaws, C. L. (1996), Appendix D—Critical properties and acentric factor for inorganic compounds and elements inorganic compounds and elements, in *Handbook of Thermodynamic Diagrams*, vol. 4, pp. 351–356, Gulf Prof. Publ., doi:10.1016/B978-0-88415-860-8.50036-2.

Yung, Y. L., M. Allen, and J. P. Pinto (1984), Photochemistry of the atmosphere of Titan: Comparison between model and observations, *Astrophys. J.*, *55*, 465–506, doi:10.1086/190963.

Zupan Hajna, N. (2012), Dinaric Karst: Geography and geology, in *Encyclopedia of Caves*, 2nd edn., pp. 195–203, Elsevier, Amsterdam.